Long-term experimental diagenesis of aragonitic biocarbonates: from organic matter loss to abiogenic calcite formation

Pablo Forjanes[1], María Simonet Roda[2], Martina Greiner[2], Erika Griesshaber[2], Nelson A. Lagos[3], Sabino Veintemillas-Verdaguer[4], José Manuel Astilleros[1,5], Lurdes Fernández-Díaz[1,5], Wolfgang W. Schmahl[2]

[1] Department of Mineralogy and Petrology, Universidad Complutense de Madrid, Madrid, 28040, Spain
[2] Department of Earth and Environmental Sciences, Ludwig-Maximilians-Universität, Munich, 80333, Germany
[3] Centro de Investigación e Innovación para el Cambio Climático, Universidad Santo Tomás, Santiago, Chile
[4] Instituto de Ciencia de Materiales de Madrid (ICMM, CSIC), Madrid, 28049, Spain
[5] Instituto de Geociencias (IGEO), (UCM, CSIC), Madrid, 28040, Spain

Correspondence to: Lurdes Fernández-Díaz (lfdiaz@geo.ucm.es) and Pablo Forjanes (pforjane@ucm.es)

Abstract. Carbonate biological hard tissues are valuable archives of environmental information. However, this information can be blurred or even completely lost as hard tissues undergo diagenetic alteration. This is more likely to occur in aragonitic skeletons because bioaragonite commonly transforms into calcite during diagenesis. For reliably using aragonitic skeletons as geochemical proxies, it is necessary to understand in depth the diagenetic alteration processes that they undergo. Several works have recently investigated the hydrothermal alteration of aragonitic hard tissues during short term experiments at high temperatures (T > 160ºC). In this study, we conduct long term (4 and 6 months) hydrothermal alteration experiments at 80ºC using burial-like fluids. We document and evaluate the changes undergone by the outer and inner layers of the shell of the bivalve *Arctica islandica*, the prismatic and nacreous layers of the hard tissue of the gastropod *Haliotis ovina*, and the skeleton of the coral *Porites* sp. combining a variety of analytical tools (X-ray diffraction, thermogravimetry analysis, laser confocal microscopy, scanning electron microscopy, electron backscatter diffraction and atomic force microscopy). We demonstrate that this approach is the most adequate to trace subtle, diagenetic alteration-related changes in aragonitic biocarbonate structural hard materials. Furthermore, we unveil that the diagenetic alteration of aragonitic biological hard tissues is a complex multi-step process where major changes occur even at the low temperature used in this study, well before any aragonite into calcite transformation takes place. Alteration starts with biopolymer decomposition and concomitant generation of secondary porosity. These processes are followed by abiogenic aragonite precipitation that partially or totally obliterates the secondary porosity. Only subsequently, occurs the transformation of the aragonite into calcite. The kinetics of the alteration process is highly dependent on primary microstructural features of the aragonitic biomineral. While the skeleton of *Porites* sp. remains virtually unaltered for the entire duration of the conducted experiments, *Haliotis ovina* nacre undergoes extensive abiogenic aragonite precipitation. The outer and inner shell layers of *Arctica islandica* are significantly affected by aragonite transformation into calcite. This transformation is extensive for the prismatic shell layer of *Haliotis ovina*. Our results suggest

that the majority of aragonitic fossil archives are overprinted, even those free of clear diagenetic alteration signs. This finding may have major implications for the use of these archives as geochemical proxies.

Key words: Carbonates, Biominerals, Aragonite, Diagenesis, Diagenetic tracers: FE-SEM, EBSD, AFM.

40   **1 Introduction**

Calcium carbonate hard tissues are valuable geochemical proxies for deciphering past climate dynamics and environmental change. However, the greatest challenge that these biological archives face lies in their capacity to retain their pristine signature after the death of the calcifying organism, since from this moment, the skeletons become highly prone to alteration. The original

45   microstructure and chemical composition of the biocarbonate structural hard tissue can become partially, in the best case, to totally, in the worst case, obliterated; and so does the environmental-derived information recorded in it (Brand, 1989; Swart, 2015; Casella et al., 2018, Pederson 2019a, 2019b, 2020).

Biocarbonate structural materials are composites of biopolymers and calcium carbonate mineral phases (mostly calcite and/or

50   aragonite, rarely and much less abundantly vaterite) (Weiner and Dove, 2003). The alteration of biocarbonate hard tissues is influenced by both external, environment-related, and internal, archive-related, factors. Main external factors are: alteration time, the degree of geochemical disequilibrium with the environment, the physicochemical conditions in the depositional environment, the porosity and permeability of the sediments, the chemical composition of the pore fluids and the fluid-rock ratio, among others (Pederson et al., 2019a, 2019b, 2020). On the other hand, some internal factors that influence the alteration

55   kinetics of the calcium carbonate skeletons are the concerned carbonate phase, the original microstructure and texture of the mineral component, the fabric, amount and distribution of the organic matter within the composite hard tissue, etc. (Gaffey 1988; Gaffey et al., 1991, Casella et al., 2018, Pederson et al., 2020). At the conditions that prevail in natural diagenetic environments, calcite is the stable calcium carbonate polymorph while aragonite is the more soluble, thermodynamically metastable phase (Plummer and Mackenzie, 1974; Plummer and Busenberg, 1982; Sass et al., 1983; Walter and Morse, 1984;

60   Bischoff et al., 1987, 1993; Redfern et al., 1989; Navrotsky, 2004; Morse et al., 2007; Gebauer et al., 2008, Radha et al., 2010; Gebauer and Cölfen, 2011; Radha and Navrotsky, 2013). In the presence of an aqueous phase, aragonite crystals can transform into calcite through a coupled dissolution-crystallization reaction. The progress of the reaction is driven by the difference in solubility between the two carbonate phases and is facilitated by the generation of porosity (Berner, 1975; Bischoff, 1969; Bischoff, 1968; Fyfe and Bischoff, 1965; Cardew and Davey, 1985; Mucci et al., 1989; Putnis and Putnis, 2007; Putnis, 2009,

65   Ruiz-Agudo et al., 2014; Sun et al., 2015). The result of this dissolution-crystallization reaction is the formation of calcite pseudomorphs after aragonite that consist of blocky calcite crystals (Perdikouri et al., 2008, 2011, 2013). It is noteworthy that biogenic calcite also is metastable with respect to abiogenic calcite, and that calcite biominerals may undergo dissolution-

recrystallization reactions that result in the diagenetic overprint of their isotopic notations, as was recently demonstrated experimentally (Bernard et al., 2017; Cisneros-Lázaro et al. 2021, 2022).

70

The metastable nature of aragonite explains that aragonitic skeletons have a lower potential of becoming preserved in the geologic record, relative to their calcitic counterparts (James et al., 2005; Cherns and Wright, 2011; Cherns et al., 2011, Janiszewska et al., 2018; Wright et al., 2003; Wright and Cherns 2004). Lowenstam (1954) and Hallam and O'Hara (1962) estimated that, during diagenesis, most aragonitic carbonates would be replaced by calcite within a few to thousands of years.

75 However, under low-temperature regimes, in shallow environments enriched in organic matter, the transformation of aragonite into calcite is precluded and the progress of diagenetic alteration is restricted to its very first stages (Hall and Kennedy, 1967; Seuss et al. 2009; Janiszewska et al., 2018). The resulting structural and chemical changes between the pristine and altered skeletons are then very subtle and difficult to trace. In this work we aim to disclose the subtle microstructural and chemical changes undergone by aragonitic hard tissues during low-temperature/long-time hydrothermal alteration. We conducted long-

80 term (4 and 6 months) hydrothermal alteration experiments at 80°C with burial-mimicking Mg-rich waters. Aiming to understand the influence of bioaragonite architecture in the kinetics of hydrothermal alteration we investigated the alteration response of three very different biocarbonate skeletons: (i) the granular aragonite that forms the shell of the bivalve *Arctica islandica*, (ii) the prismatic and columnar nacreous aragonite that comprises the shell of the gastropod *Haliotis ovina* and (iii) the acicular, fibrous aragonite that builds up the skeleton of the coral *Porites* sp. By comparing the hydrothermal overprint

85 undergone by these microstructures after prolonged alteration at 80ºC (this study) and after much shorter alteration at 175 °C (Casella et al., 2018) we identify better early hydrothermal alterations steps and improve our understanding regarding the role of temperature and time in the progress of alteration and overprint. This study demonstrates that a combination of analytical tools and evaluation techniques (TGA and XRD measurements, Rietveld analysis of XRD data, EBSD measurements and grain size statistical evaluation, laser confocal microscopy, FE-SEM and AFM imaging) provides the ideal set of data to

90 pinpoint the structural changes caused by the hydrothermal and/or diagenetic alteration of biological hard tissues, even the subtle changes that are difficult to address, that mark the very first steps of biocarbonate microstructural reorganization.

2 Material and Methods

2.1 Materials

95 Three aragonitic hard tissues from animals with very different microstructures were chosen for this study. Shells of the modern bivalve *Arctica islandica* were collected from Loch Etive in Scotland (United Kingdom). Adult specimens of the gastropod *Haliotis ovina* were obtained at Heron Island in Queensland (Australia). Samples of the scleractinian coral *Porites* sp. were collected at Moorea, French Polynesia (France).

2.2 Methods

2.2.1 Hydrothermal Alteration Experiments

For the alteration experiments, pieces of the hard tissues were cut into slices with a diamond 6-inch saw (Hi-Tech-Diamond) and cut subsequently into three rectangular 2 cm x 1 cm fragments (Fig. A1). All three segments were hydrothermally altered. Hydrothermal alteration experiments were carried out mimicking diagenetic conditions regarding fluid temperature and composition. The used fluid composition (100 mM NaCl + 10 mM MgCl$_2$) simulates the fluid present at the burial diagenetic realm. The composition of the fluid was identical to that previously used by Casella et al., (2017, 2018) and Pederson et al., (2019a; 2019b; 2020) in their hydrothermal alteration experiments.

For all alteration experiments, 3 pieces of the pristine skeletons of modern *Arctica islandica* (0.8g/piece), *Haliotis ovina* (0.2g/piece) and *Porites* sp. (0.1g/piece) were placed into a polytetrafluoroethylene (PTFE) vessel together with 10 mL of the Mg-rich burial aqueous solution (Water/rock ratio of 4.16, 16.66 and 33.33, respectively) (Casella et al., 2017, 2018). The PTFE vessels were then sealed with a PTFE cover and inserted into stainless-steel autoclaves, which were subsequently sealed, and kept in an oven at 80ºC for 4 and 6 months. After hydrothermal alteration, the autoclaves were recovered from the oven, cooled down at room temperature (20ºC) and opened. The recovered altered samples were dried overnight at 40ºC in a furnace. Subsequently, the samples were prepared for further analysis. For all the hydrothermal experiments, it was ensured that the shell pieces selected for alteration were taken from the same valve to avoid differences in the alteration caused by metabolic effects.

2.2.2 Structural Hard Tissue Characterization

X-ray diffraction (XRD) and Rietveld analysis

One of the three pieces of every altered sample was crushed in an agate mortar and measured with powder X-ray diffraction (XRD) for phase composition evaluation. The analysis was performed using Cu-Kα1 radiation in reflection geometry on a General Electric Inspection Technologies XRD3003 X-ray diffractometer with an incident-beam Ge111 focussing monochromator and a Meteor position-sensitive detector (GE Inspection Technology GmbH). The obtained XRD data were evaluated with Rietveld analysis, using the software FULLPROF (Rodriguez-Carvajal, 2001) and the CIF structural data from Markgraf and Reeder (1985) for calcite and from Jarosch and Heger (1986) for aragonite, from the Crystallography Open Database (COD 2017). The above-described data evaluation procedure was applied to all pristine as well as altered samples.

Thermal Gravimetric Analysis (TGA)

The sample that was used for XRD measurements was recovered from the XRD holder and was further used for TGA measurements for the determination of organic matter content within the pristine and altered sample. TGA measurements were conducted with a Q500 TGA. The samples were heated from room temperature to 1000ºC at a constant rate of 5ºC per minute in a flowing-air atmosphere. 25 mg of powder of every sample were used for TGA analysis.

135

2.2.3 Imaging Techniques

Laser Confocal Microscopy

Overview images for the visualization of the different microstructures within a shell or skeletal element were taken with a 140 Keyence 3D laser scanning confocal microscope (VK-X1000 series). The second shell or skeleton segments were embedded in epoxy resin and polished down with eight sequential polishing steps for obtaining a highly even sample surface. Laser confocal microscopy imaging was conducted on uncoated samples.

Atomic Force Microscopy (AFM)

145

The sub-micrometre and nanometre structure of the shells and skeletal elements was scanned with AFM. AFM imaging was done in non-coated, epoxy-embedded and highly polished sample surfaces. Samples were imaged in contact mode with a JPK NanoWizard II AFM using silicon nitride cantilevers. Scans of lateral and vertical deflection traces were analysed with the NanoWizard® IP image processing software by using the "gold" scale for colour. The lateral and vertical deflection traces are 150 the result of the interaction between the cantilever tip and the sample surface. Height traces were used to generate 3D models of the nanoscale topography of some of the samples.

FE-SEM imaging and EBSD measurements

155 To visualize major microstructural elements in the pristine and the altered samples, the aragonitic hard tissues were imaged with FE-SEM and analyzed with EBSD. The remaining piece of the altered samples, together with pristine skeletons, were embedded into epoxy resin and polished with several mechanical grinding and polishing steps down to a grain size of 1µm. Subsequently, the samples were polished with an alumina (particle size ~0.06 µm) containing suspension in a vibratory polisher (VibroMet 2; Buehler) for 2 hours. For EBSD measurements the samples were coated with 5 to 6 nm of carbon, for 160 FE-SEM imaging, additionally with 8 to 10 nm of Pt/Pd.

FE-SEM imaging and EBSD measurements were carried out in a Hitachi SU5000 field emission SEM, equipped with an Nordlys Oxford EBSD detector. The SEM was operated at 20 Kv and the Kikuchi diffraction patterns were indexed with the

Oxford Instruments AZTec and CHANNEL 5 HKL software (Schmidt and Olesen, 1989; Randle, 2000). Information obtained from EBSD measurements is presented here as band contrast measurement images and as colour-coded crystal orientation maps with their corresponding pole figures; the latter giving either individual data points or, in the contoured version, the strength of the clustering of poles (Half width of 5º and cluster size of 3º).

EBSD band contrast gives the signal strength of the EBSD-Kikuchi diffraction pattern and is displayed as a grey-scale component in a map. The strength of the EBSD signal is high when a crystal is detected (bright in the map), whereas it is weak or absent when a polymer, such as organic matter or epoxy resin, is scanned (dark/black on the map). Crystal co-orientation statistics are derived from Kikuchi diffraction patterns measured at each image pixel of an EBSD map. Crystal co-orientation is given by the MUD value (multiple of uniform (random) distribution). A high MUD indicates high crystal co-orientation, while low MUD values reflect low to random crystallite or/and mineral unit co-orientation. Pole figures are stereographic projections of the orientations of crystallographic axes or plane normals measured at all pixels of an EBSD map.

The term texture relates to the distribution of crystal orientations within a material and is illustrated by pole figures, showing either colour-coded orientation data or contoured versions of density distributions of c- and a*-axes poles. A fibre texture or axial texture is present when the measured orientations have a one-dimensional orientation order. For brachiopod shell calcite usually the c-axes of the individual crystals are co-oriented, showing a cluster concentrated around one particular direction in the {001} (= c-axis) pole figure, whereas the {100} (= a*-axes) scatter in orientation around the great circle perpendicular to the c-axis (Simonet Roda et al., 2019; 2022). A three-dimensional texture or three dimensional orientational order is present when all crystallographic axes in the investigated map are co-oriented, such that there is a concentrated cluster of data points around one particular direction in the c-axes pole figure but also distinct clustering on the great circle perpendicular to this direction in the a*-axes pole figure. Since, for calcite, the c-axis is a unique direction and bears the $\bar{3}$ symmetry axis, there are six maxima in the a*-axis pole figure. However, only three of those are usually visible in the pole figure because data of only one hemisphere of the stereographic projection are displayed. The term microstructure refers to the sum of grains, their sizes, morphologies, modes of interlinkage, co- and misorientations and is shown with coloured EBSD maps. Similar colours visualize similar crystal orientations, different colours indicate differences in crystal orientation.

Grain area/size statistical evaluation

EBSD measurements allow us to distinguish between individual grains and, hence, to obtain grain related parameters such as grain area and grain boundaries. A grain in an EBSD map is defined as a region that is completely surrounded by boundaries across which the misorientation angle relative to the neighbouring grains is larger than a critical value. In this study we use a critical misorientation value of 2º. The latter was determined empirically and is appropriate for carbonate biological hard tissues (Griesshaber et al., 2013). To evaluate grain size distributions, we chose grain clusters with a class width of 0.10 μm^2

for aragonite nacre tablets and 0.15 μm^2 for the other aragonitic microstructures. In this study we plotted the relative frequency of every cluster with respect to the total amount of grains (%) relative to grain area/grain size (μm^2).

200

3 Results

3.1 The pristine microstructure of *Arctica islandica*, *Haliotis ovina* and *Porites* sp. skeletons.

205 The pristine skeletons of *Arctica islandica*, *Haliotis ovina* and *Porites* sp. consist entirely of aragonite according to XRD measurements and Rietveld analysis (Fig. A2 and A4 from Casella et al., 2018) and have an organic matter content that varies significantly for the different species. Organic matter concentration in the investigated hard tissues was determined with TGA analyses (Fig. A3).

210 The shell of the bivalve *Arctica islandica* is comprised of irregularly shaped micrometre-sized aragonite crystals which are interconnected by a network of biopolymer fibrils (Casella et al., 2017). Annual growth lines are frequent (Fig. A4 and A5). Aragonite crystals are unstructured and show a poor co-orientation strength according to EBSD measurements and data analysis (MUD = 8). This is the case for the outer region of the shell, next to seawater. Contrarily, the crystals which constitute the innermost layer of the skeleton, closer to the soft tissue of the animal, have a crossed lamellar microstructural arrangement,
215 with higher MUD values (59) (Fig. 1 and A6). Despite having a densely packed aragonitic microstructure, the pristine skeleton of *Arctica islandica* contains primary porosity. This porosity is more abundant in the outer regions of the shell and decreases towards the inner portions (Fig. A4 and A5). TGA analysis of the pristine shell of *Arctica islandica* show that the amount of organics in the shell varies between 1.8 wt. % in the inner shell and 2.2 wt. % in the outer shell portion, respectively (Fig. A3). Despite the differences in shell microstructure, aragonite nanostructure is relatively homogeneous throughout the pristine
220 *Arctica islandica* shell. AFM images show that aragonite has a slightly rough surface, made up of spherical or near-spherical aragonite subunits of less than 100 nm width (yellow star in Fig. 2).
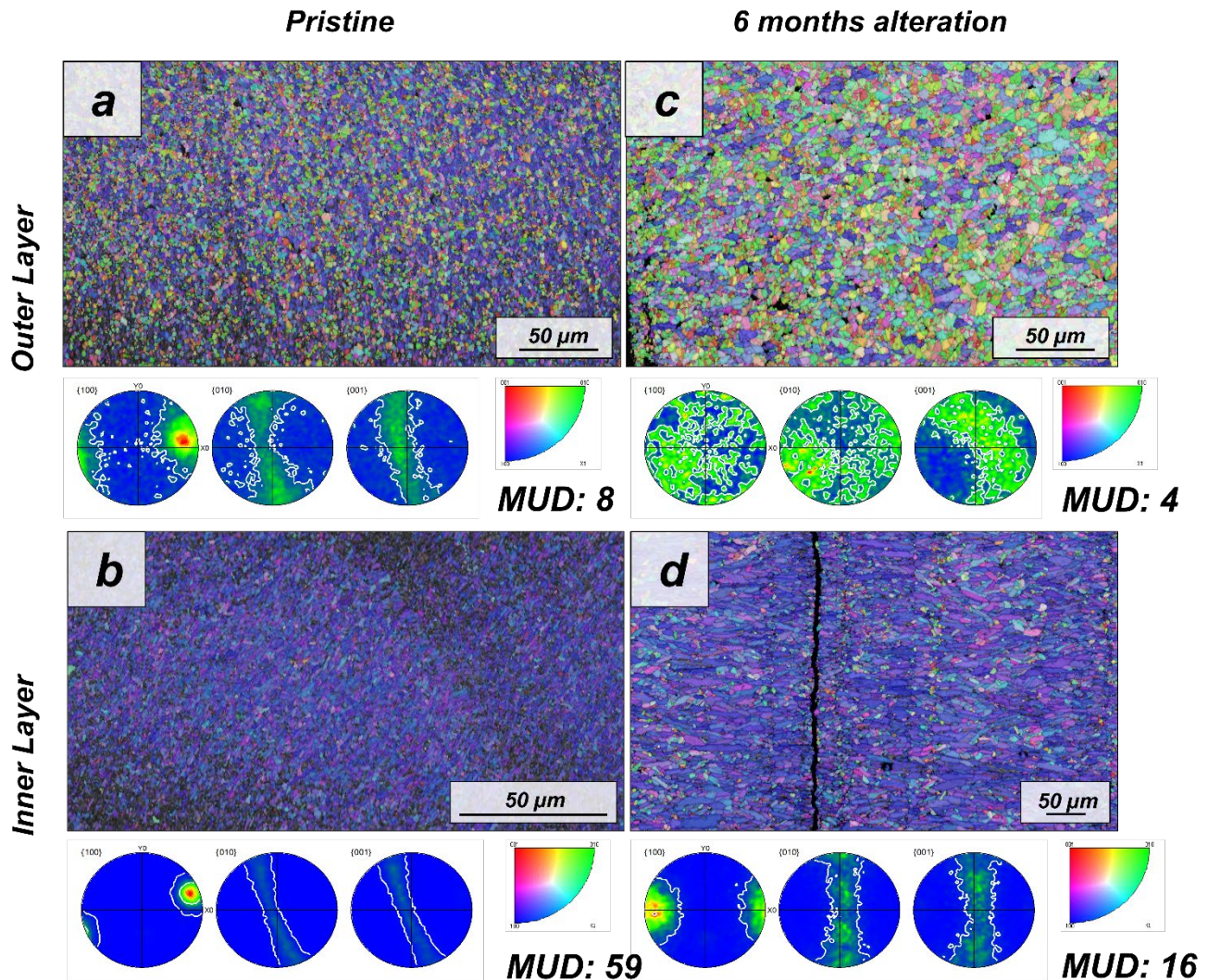
Figure 1. EBSD colour-coded orientation maps with their corresponding pole figures depicting aragonite microstructure and texture in: (a-b) pristine and (c-d) altered shells of the bivalve *Arctica islandica*. The strength of crystal co-orientation is given with the MUD value for the relevant EBSD scan, which is shown for each EBSD measurement. Even though that, at the applied hydrothermal alteration, new abiogenic calcite formation does not yet take place, the strong decrease in MUD values between the pristine and the altered samples indicates reorganization of the microstructure through new, abiogenic, aragonite formation.
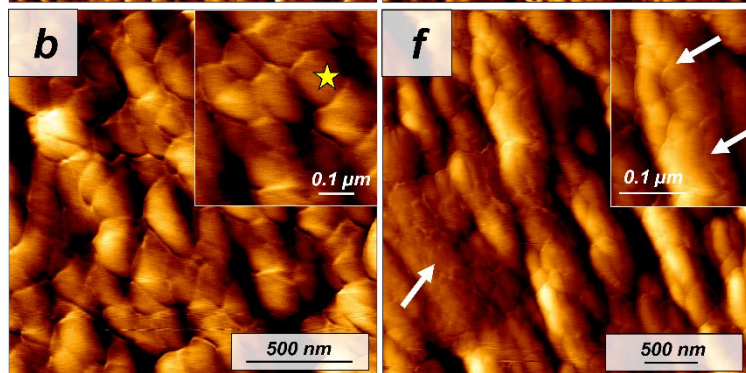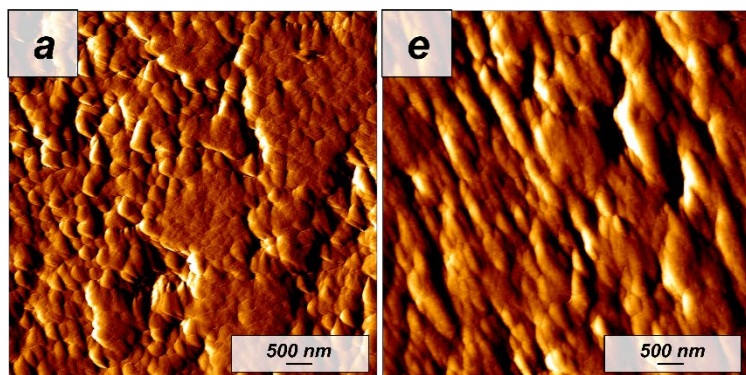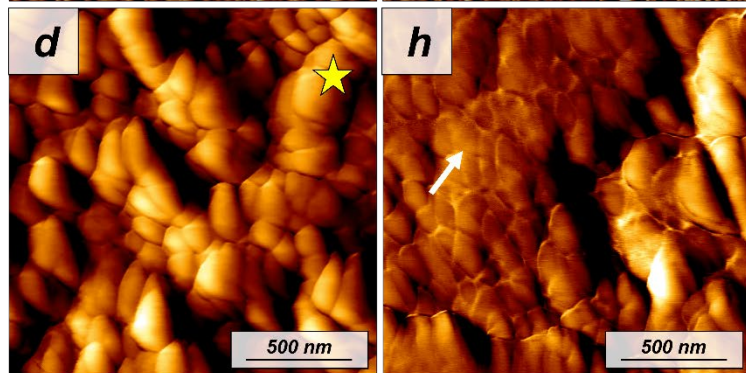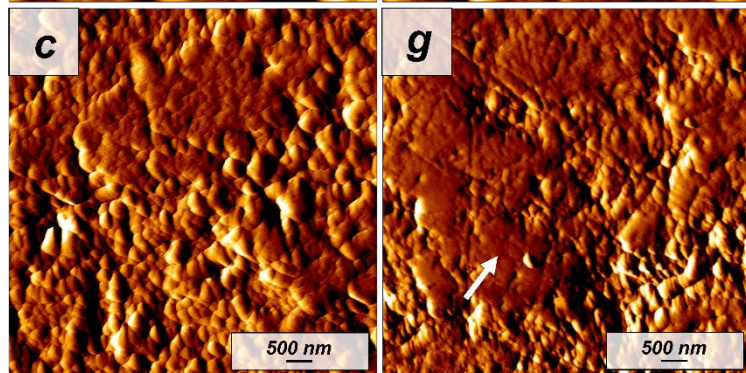
Figure 2. Vertical deflection AFM images of: (a-d) pristine and (e-h) altered shells of the bivalve *Arctica islandica*. Pristine shells of *Arctica islandica* are composed of two aragonitic layers formed by aragonitic subunits of less than 100 nm in size (yellow star in Fig. 2b and 2d; shell constituent units). Insets in figures 2b and 2f show a closer view of these units. Hydrothermal alteration induces amalgamation of the subunits (white arrows in Figs. 2e to 2h).

The pristine shell of the gastropod *Haliotis ovina* shows two microstructural arrangements. The outer layer, that points towards seawater, is composed of aragonite prisms while the inner layer, closer to the soft tissue of the animal, is composed of aragonitic nacre tablets (Fig. A7 and A8). The latter are arranged in columns. The aragonite prisms have an irregular shape and show a gradation in size, such that the smaller crystals are in the outermost regions of the shell, in contact with the seawater, and the largest aragonite prisms are close to or at the transition to the nacreous shell portion (Fig. A9a). The nacre tablets, on the other hand, have an average thickness of 430 to 500 nm (Fig. A9b). There is a very sharp boundary between the two microstructures. Aragonitic nacre represents about 80 to 85% of the shell of *Haliotis ovina*, while the aragonitic prisms account for the remaining 15 to 20%. EBSD analyses demonstrate that the aragonitic nacre is highly co-oriented, with a MUD value close to 100. In contrast, the crystals that form the aragonitic prisms show lower crystal co-orientation strength. MUD values scatter between 19 and 31 (Fig. 3 and A10). TGA analysis of the pristine shell of *Haliotis ovina* show that the amount of organics in the shell is 3.1 wt. %. The nanostructures of the two microstructural arrangements of pristine *Haliotis ovina* are depicted in Fig. 4. Aragonite prisms have a rough surface composed of aragonite subunits with sizes ≤ 100 nm (yellow star in Fig. 4b). Aragonite nacre tablets are formed of smaller aragonitic subunits, separated from each other by linear continuous divisions, the sites where the organic matter is concentrated. A 3D model of the nacre surface derived from height AFM measurements is given in Fig. 5 and shows that this microstructure has a topography in which the divisions between the different tablets, that is, the place where the organic matter is concentrated, stands out topographically (30 nm on average) above the mineralized areas.

Pristine

6 months alteration

Boundary

Aragonite Nacre

Aragonite Prisms
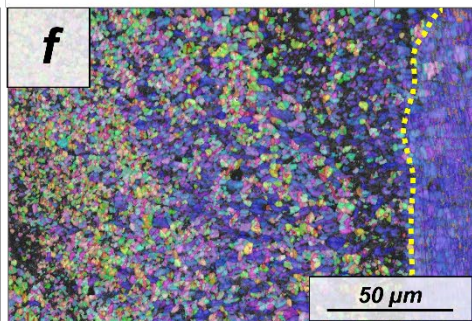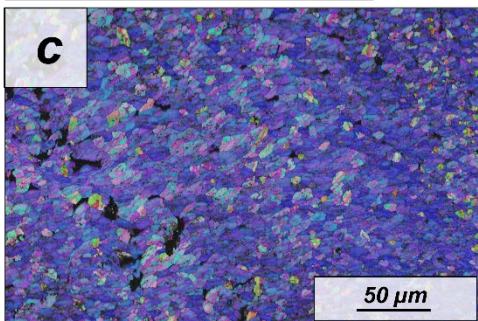
a

d

Calcite

50 µm

50 µm

Pole Figure from the Aragonite Nacre

MUD: 133

Pole Figure from the Inorganic Calcite

MUD: 192

Pole Figure from the Aragonite Prisms

MUD: 33

Pole Figure from the Aragonite Prisms

MUD: 13

b

e

50 µm

50 µm

Pole Figure from the Aragonite Nacre

MUD: 93

Pole Figure from the Aragonite Nacre

MUD: 220

c

f

50 µm

50 µm

Pole Figure from the Aragonite Prisms

MUD: 19

Pole Figure from the Aragonite Prisms

MUD: 8

255
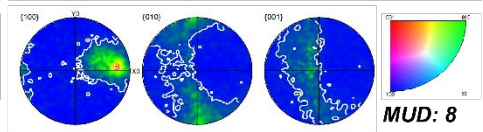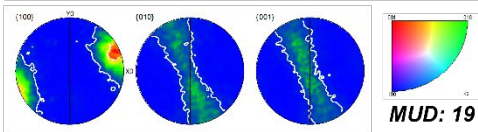
Figure 3. EBSD colour-coded orientation maps with their corresponding pole figures depicting the microstructure and texture of biogenic aragonite of the (a-c) pristine and (d-f) altered shells of the gastropod *Haliotis ovina*. The strength of crystal co-orientation is given with the MUD value, which is shown for each EBSD scan. Hydrothermal alteration of *Haliotis ovina* induces the replacement of large parts of the prismatic aragonite by non-biogenic calcite concomitant to a decrease of the MUD value of the untransformed aragonite prisms. Though the nacreous layer is not replaced by calcite, its MUD value increases from 93 to 220.

Pristine

6 months alteration

Aragonite Prisms of Haliotis ovina.
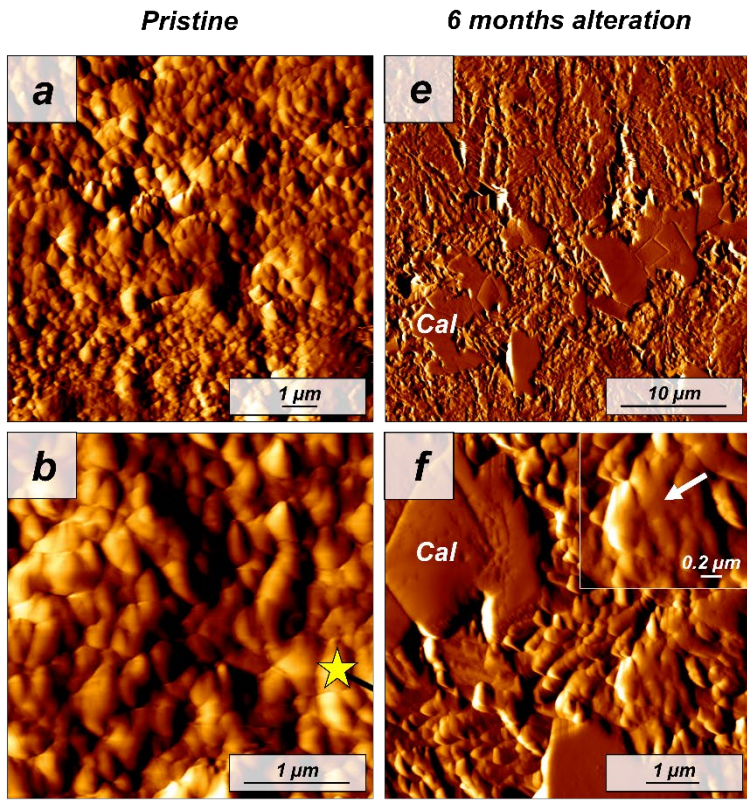
Aragonite Nacre Tablets of Haliotis ovina.
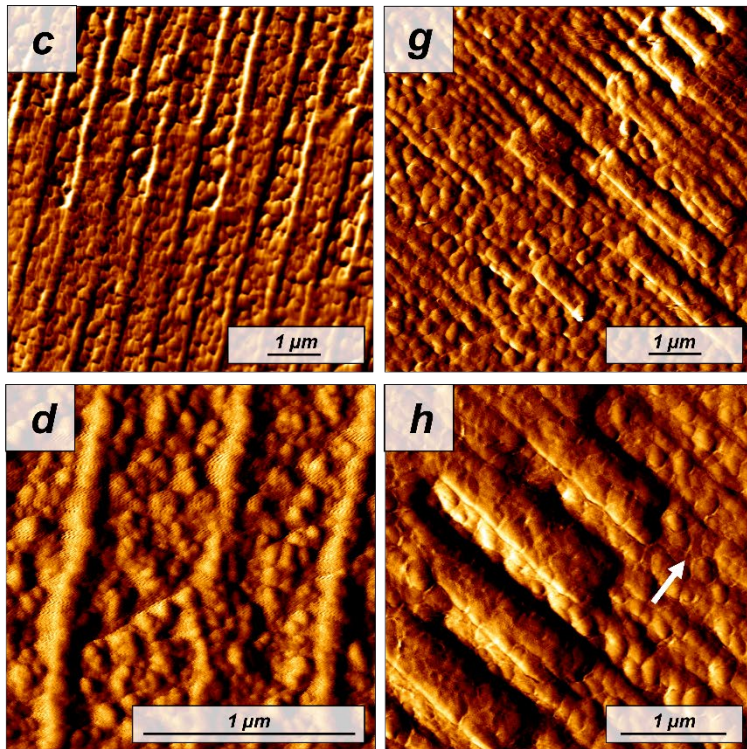
Figure 4. Vertical deflection AFM images depicting: (a-d) the pristine and (e-h) altered shells of the gastropod *Haliotis ovina*. The pristine shell of *Haliotis ovina* is composed of two layers: (a,b) A prismatic shell layer (yellow star; shell constituent units) and a (c,d) nacreous inner portion consisting of an assembly of nacre tablets, formed by small rounded aragonitic subunits. (e-h) Upon hydrothermal alteration, abiogenic calcite crystals, with their characteristic rhombohedral shape, form in the former biogenic prismatic layer. In both layers, we observe an amalgamation of mineral units (see inset in figure 4f). In the nacreous layer, boundaries of individual nacre tablets become blurred (white arrow in h). Cal: calcite crystals.
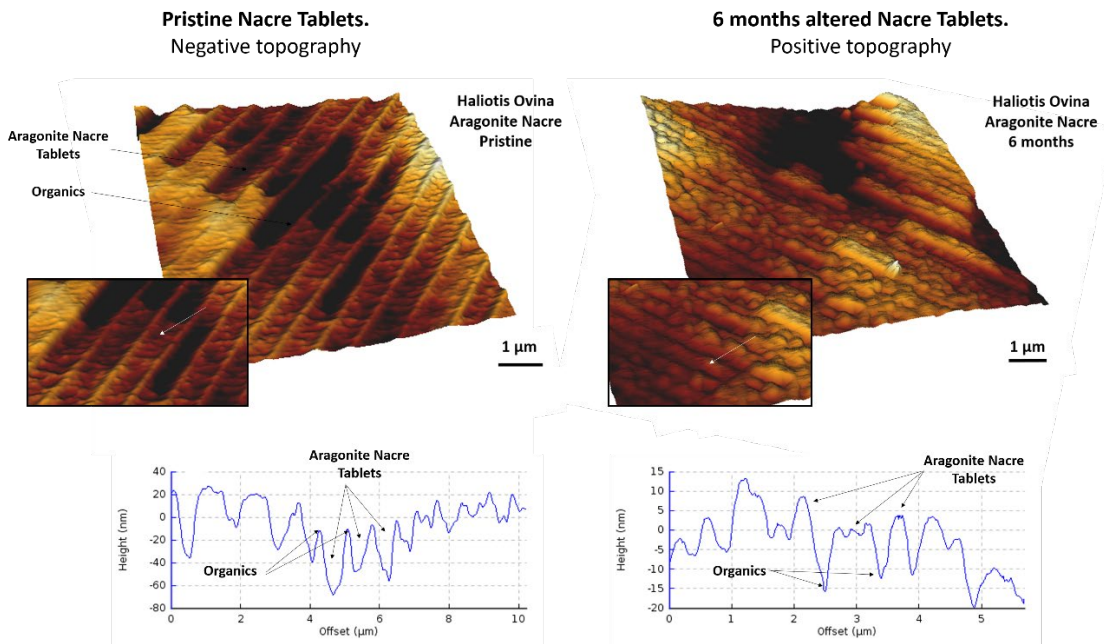
Figure 5. 3D surface reconstruction of height AFM measurements of aragonitic nacre tablets for: (a) pristine and (b) altered shell segments of the gastropod *Haliotis ovina*. In the pristine shell, the organic membranes that separate adjacent tablets have a positive relief, while in the altered shell analogue a dramatic structural change is observable. At the site of the organic membrane we find a depression.

The modern skeleton of the scleractinian coral *Porites* sp. has a very compact microstructure in which spherulitic aragonitic units formed by acicular crystals grow radially around the calcification centres, the places where mineral nucleation starts (Fig. A11 and A12). EBSD data analyses show that acicular aragonite in *Porites* sp. has an average MUD value of 10 (Fig. 6 and A13). TGA analysis of the pristine *Porites* sp. skeletons show that the amount of organics in the sample is 2.1 wt. %. AFM

images of the pristine skeleton of *Porites* sp. show that the aragonitic acicular crystals which build up this microstructure are composed of aragonitic subunits of approximately 0.1 µm width (Fig. 7).
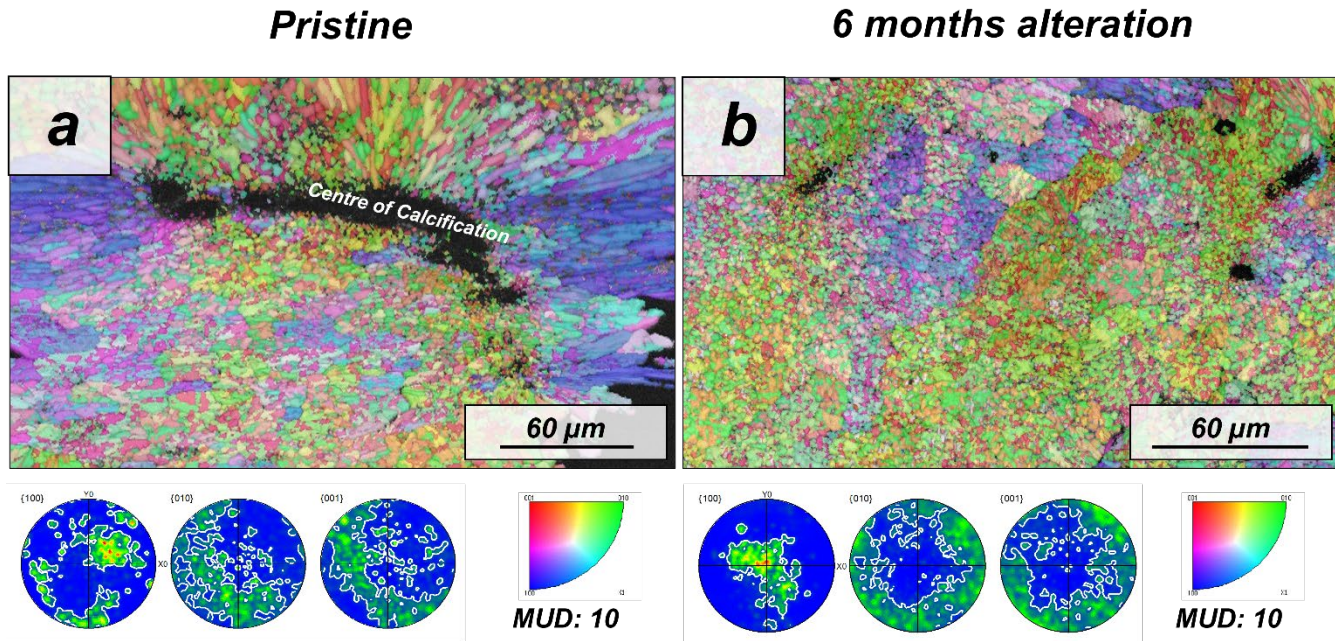
Figure 6. Colour-coded orientation maps with their corresponding pole figures derived from EBSD scans depicting the microstructure and texture of: (a) pristine and (b) altered coral, *Porites* sp., skeletons. Crystal co-orientation is given by the MUD value. No major changes can be observed between the pristine and the altered skeletal elements. However, we do not discard that the alteration may have produced variations in the microstructure of Porites sp. that could not be detected by EBSD. The low co-orientation of the aragonite crystals in the pristine sample makes it difficult to see variations after alteration.

Pristine **6 months alteration**
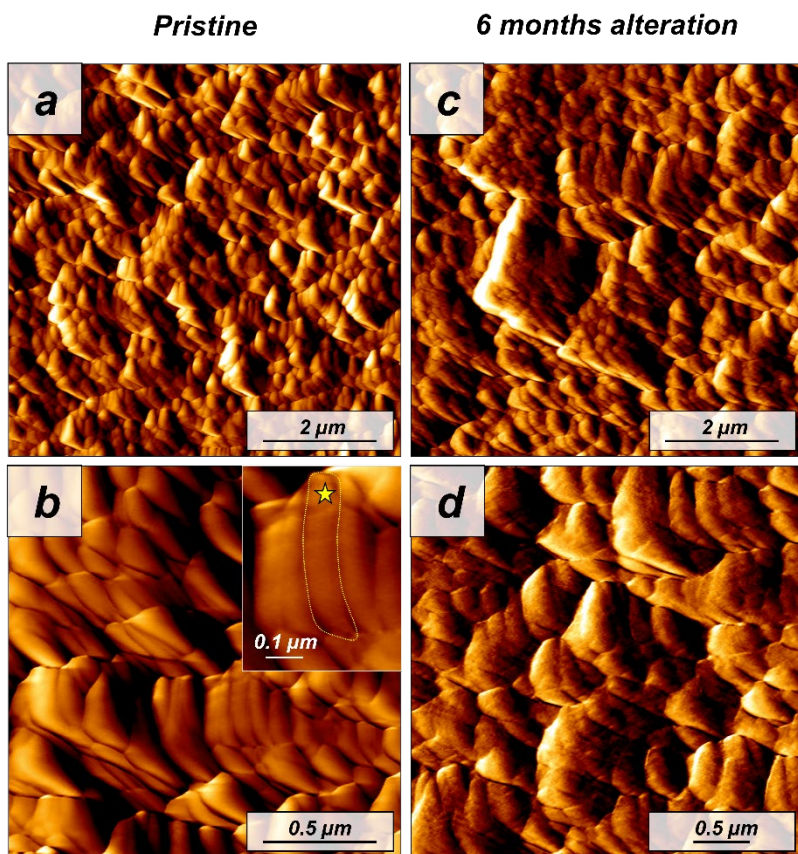
295

Figure 7. Vertical deflection AFM images of (a-b) pristine and (c-d) altered *Porites* sp. samples. The coral microstructure is formed by acicular aragonite crystals which, in turn, are composed of minute roundish subunits (yellow star in the inset from figure 7b). Hydrothermal alteration experiments conducted in this study did not induce any significant change to the submicro

300   to nanostructure of the coral skeleton.

3.2 The hydrothermally altered microstructures of *Arctica islandica*, *Haliotis ovina* and *Porites* sp. skeletons.

The interaction of the hard tissues of *Arctica islandica*, *Haliotis ovina* and *Porites* sp. with a burial-mimicking fluid for up to

305   6 months at 80°C produces little to no transformation of the biogenic aragonite into abiogenic calcite, according to Rietveld analysis derived from XRD data (Fig. 8a, A2 and A14). Thus, after 6 months interaction with the burial fluid the total amount of calcite in the altered samples is approximately 16 wt. % in *Haliotis ovina*, 1 wt. % in *Arctica islandica* and less than 0.1 wt. % in *Porites* sp. It is remarkable that, even though, *Haliotis ovina* contains 16 wt. % of calcite after 6 months of alteration, this value is still only 0.8 wt. % after 4 months of alteration.

310 TGA measurements show a reduction in the organic matter content of ~ 30 wt. % in *Arctica islandica* (from 2 wt. % to 1.3 wt. %), ~ 20 wt. % in *Haliotis ovina* (from 3.06 wt. % to 2.47 wt. %) and ~ 7 wt. % in *Porites* sp. (from 2.10 wt. % to 1.96 wt. %) (Fig. 8b and A3).
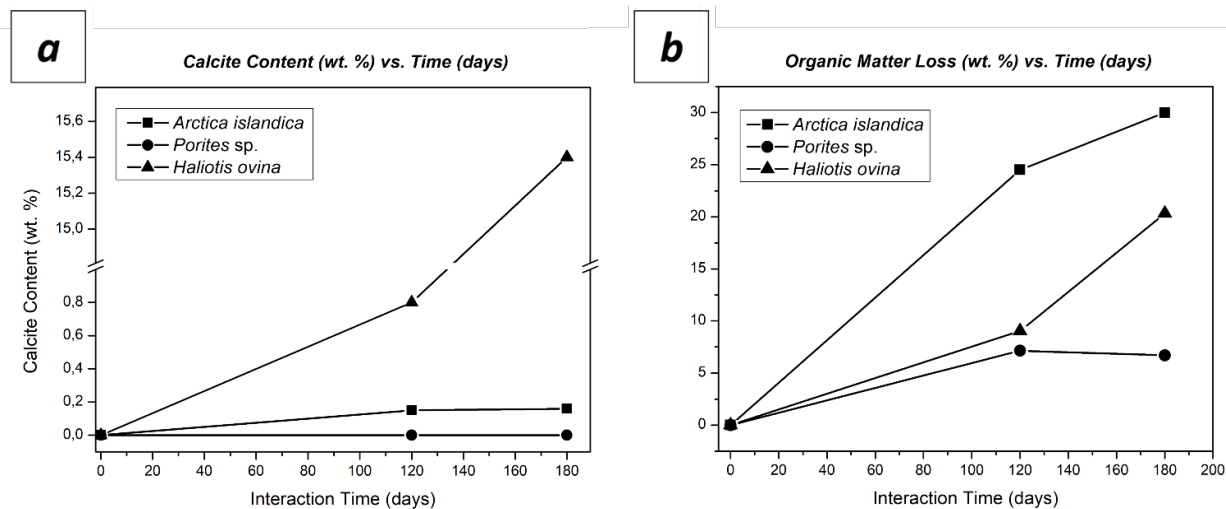
315

Figure 8. (a) Calcite content obtained from Rietveld analysis derived from XRD data and (b) organic matter loss measured with TGA with increasing alteration time. The influence of the individual aragonitic microstructure on both parameters is remarkable.

320 Laser confocal microscopy imaging was used to obtain overview images of sample surfaces to visualize main differences between the pristine and the altered samples (Fig. A4, A7 and A11). In the case of *Haliotis ovina*, new calcite crystals can be observed at the change-over from aragonite prisms to aragonite nacre tablets.

The microstructural evolution of the altered samples was followed with FE-SEM and EBSD measurements and the submicro-
325 to nanostructural evolution of the altered samples was recorded with AFM imaging. FE-SEM images of *Arctica islandica* shells, altered for 6 months, show no major changes, in comparison to the pristine samples (Fig. A5). Contrarily, EBSD measurements show a significant drop in the MUD value for the aragonite crystals that compose the shell of *Arctica islandica*. Thus, after 6 months interaction with the burial fluid, the MUD value of the outer layer of *Arctica islandica* shells drops from 8 to 4, while the MUD value of the crossed lamellar aragonite along the inner layer of the shell drops from 59 to 16, respectively
330 (Fig. 1). AFM images taken on the altered shell of *Arctica islandica* show that crystal amalgamation occurs in the aragonite subunits of both shell layers (white arrows in Fig. 2).

For *Haliotis ovina* shells, FE-SEM images show large calcite crystals growing at the transition from nacreous to prismatic aragonite (Fig. A8). The calcite crystals have a flat surface and are devoid of pores. Aragonite nacre tablets are subject to crystal/tablet amalgamation, a feature that is well observable, as the boundaries between the different tablets become increasingly blurred with elapsing interaction time (Fig. A8). FE-SEM, laser confocal microscopy imaging and EBSD measurements show that the large calcite crystals (more than 100 microns) are concentrated at the boundary between the two aragonitic microstructures. These crystals appear very bright in the band contrast map (Fig. A10) and show individual MUD values above 600, a MUD value that is close to that of calcite single crystals precipitated from solution (Nindiyasari et al., 2014a; 2014b). The remaining, not transformed, aragonite prisms undergo a significant drop in their MUD value, from 19 in the pristine shell to 8, in the sample altered for 6 months. The amalgamation of the aragonite nacre tablets occurs concomitant to a rapid increase in the MUD value for this particular microstructure, which rockets from 91 in the pristine shell to 220 in the altered one. AFM images taken on the altered shells of *Haliotis ovina* show new abiogenic calcite crystals growing within the aragonite prisms (Fig. 4). These calcite crystals have a much smoother surface than the surface of the biogenic minerals. The newly formed calcite crystals have straight edges and, in some cases, allow us to distinguish the characteristic rhombohedral morphology of abiogenic calcite. The formation of abiogenic calcite takes place concomitant to an amalgamation of the aragonitic prisms, similar to that observed in the altered shells of *Arctica islandica* (white arrow in Fig. 4f). In the case of the aragonitic nacre tablets, it can be observed that in this microstructure there is also amalgamation of aragonite crystallites. Furthermore, the 3D topographic model of the nacreous microstructure, calculated from AFM height measurements, shows that the alteration produces an inversion in the topography of the nacreous shell layer. Hence, the organic membranes between the nacre tablets, topographically elevated and well observable in the pristine shell, become depressed in the altered equivalent. (Fig. 5)

The microstructure of the stony coral *Porites* sp. shows little change upon hydrothermal alteration after 6 months interaction with a burial fluid at 80 °C. Neither FE-SEM imaging nor EBSD measurements show major differences between the pristine and the altered sample. Furthermore, the MUD value of EBSD scans made on *Porites* sp. does not change after 6 months alteration. Alike, the comparison of AFM images between pristine and altered shells, does not indicate a significant reorganization of the micro- and the nanostructure.

Statistical evaluation of grain size gained from EBSD measurements allows us to quantitatively evaluate grain size distribution in the pristine and altered samples. The area of grains was grouped into clusters of 0.15 μm^2 (0.10 μm^2 in the case of the aragonite nacre tablets for *Haliotis ovina*). These clusters are ordered by their relative frequencies and are shown in Fig. 9. This data analysis was carried out for all the microstructures investigated in this study.
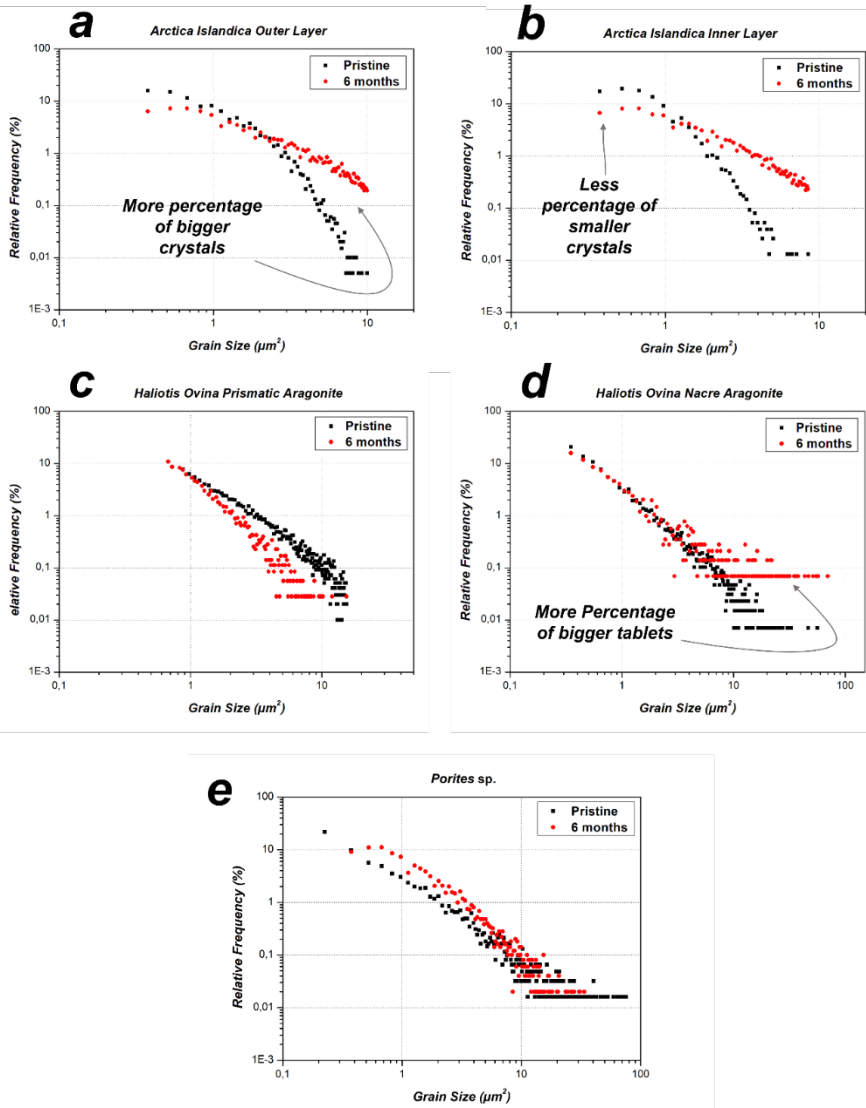
365

Figure 9. Relative frequency versus grain size/grain area for pristine and hydrothermally altered *Arctica islandica*, *Haliotis ovina* and *Porites* sp. shells and skeletal elements. (a, b): In *Arctica islandica* shells, there is a dramatic redistribution of grain size, such that the amount of smaller grains decreases, while the amount of larger grains in the shell increases. This occurs in both the outer and the inner layer of *Arctica islandica* shell. (c, d): In the shell of *Haliotis ovina*, the two layers follow a
370 different evolution with progressive alteration. The grains in the prismatic layer decrease in size, while in the nacreous layer the amount of large grains increases. (e) For the coral *Porites* sp., we do not find significant variations in grain size/grain area with progressive alteration.

For the granular microstructure of *Arctica islandica* we see significant differences between the pristine and the altered shells.

375 The observed differences are similar for both the outer and the inner layers of the animal. In the pristine shells of *Arctica islandica*, most of the grains have a small area. Thus, we find that 50.1% of the grains in the outer and 67.5% of the grains in the inner layer have an area smaller than 0.825 μm^2. In contrast, only 0.91% of the grains of the outer layer and 0.13% of the grains of the inner layer have an area greater than 4.875 μm^2. Interestingly, after 6 months of hydrothermal alteration, a reduction occurs in the number of small grains which is coupled to an increase in the number of large grains (Table 1).

380

The two microstructures of *Haliotis ovina* shells show a very different behaviour upon hydrothermal alteration. For aragonitic prisms, there is a general decrease in grain size. The distribution of the relative frequency of the clusters is similar in the pristine and in the altered sample. However, all the clusters of the altered sample are shifted to the left, that is, towards smaller grain sizes. In contrast, for nacre tablets most of the grain area data overlaps. An exception occurs in the case of the largest

385 tablets, whose frequency increases considerably between the pristine and the altered microstructures. Accordingly, the number of nacre tablets with an area greater than 5 μm^2 increases from 5.1% in the pristine to 12.2% in the most altered shell.

For *Porites* sp., we do not observe a major change in grain size/grain area between the pristine and the most altered sample. The majority of grain-area data overlaps.

390

Table 1. Change of aragonite grain area/grain size with increasing hydrothermal alteration for inner and outer layers of *Arctica islandica*. The drastic decrease in the number of smaller grains and the concomitant increase in the number of larger grains is striking.

		Grains smaller than 0.825 μm^2	Grains bigger than 4.875 μm^2
Arctica Islandica Outer Layer	Pristine Shell	50.1%	0.91%
	6 months altered shell	27.2%	23.1%
Arctica Islandica Inner Layer	Pristine Shell	67.5%	0.13%
	6 months altered shell	28.9%	18.7%

395

400

4 Discussion

4.1 The hydrothermal alteration of aragonitic hard tissues: A multi-step process

The effect of laboratory-based hydrothermal alteration of several aragonitic biominerals has recently been studied in great detail (Ritter et al., 2017; Casella 2017; Casella 2018; Pederson et al., 2019a, 2019b, 2020). A multi-analytical approach was used to characterize the hard tissues, both pristine and after their alteration at temperatures above 100 ºC, interacting with meteoric (Mg-free) and burial-mimicking (Mg-bearing) fluids. The comparison between aragonitic microstructures of the pristine and the altered samples reveals an alteration mechanism that consists of a sequence of intermediate and consecutive steps.

Structural materials secreted by organisms are composites of biopolymers and minerals arranged in hierarchical architectures (Weiner and Dove, 2003). In these composites, mineral and organic matrices are intricately interrelated at all scale levels. This study, as well as previous works, (Casella et al., 2018, Pederson et al., 2019a, 2019b, 2020) deciphered the main intermediate steps undergone by aragonitic microstructures during hydrothermal alteration. The alteration usually starts with the degradation of the biopolymers which are incorporated into the biocarbonate material. The fabric of the organic matter within the hard tissue is either a network of organic fibrils and/or a sequence of organic membranes. The degradation of the organic matter constitutes the first step of the hydrothermal alteration process and leads to the second alteration step, which consists in the formation of a network of pores that permeate the biomineral and facilitate the circulation of the hydrothermal fluid (Casella et al., 2017; Casella et al, 2018). As a result of this rather extensive phenomenon, local dissolution of bioaragonite occurs concomitant to the precipitation of new, non-biogenic, aragonite (Casella et al., 2018). The precipitation of abiogenic aragonite is the third step of the hydrothermal alteration and results in an increase of aragonite grain size in the altered samples, relative to the size of the grains in their pristine counterparts (Casella et al., 2018). The fourth step of the hydrothermal alteration finally consists in the progressive replacement of both, biogenic as well as newly formed, non-biogenic, aragonite by new, non-biogenic, calcite crystals (Casella et al., 2017; Casella et al., 2018). In this case, the extent of the replacement depends on a variety of factors, such as temperature, time, secondary porosity network features, fluid/solid ratio; and might be stopped before a complete replacement takes place (Sandberg and Hudson, 1983). Ritter et al., (2017) have also shown that the composition of the hydrothermal fluids can induce changes in the sequence of these alteration steps.

4.2 Hydrothermal alteration kinetics modulated by bioaragonite microstructures

Temperature and time are key parameters in defining the extent of the alteration of the aragonitic hard tissues when these are exposed to interaction with hydrothermal fluids (Ritter et al., 2017; Pederson et al., 2019a). Regardless of the specific microstructure of the biocarbonate material, longer interactions and higher temperatures lead to more extensive alterations and

stronger overprints of the pristine features of the aragonitic skeletons. However, we observed that some characteristics of the pristine hard tissue make aragonitic biomaterials particularly resistant to hydrothermal alteration:

(i) The primary porosity of the biomaterial defines the initial surface area of the microstructure that is exposed to the hydrothermal fluid and can react with it. Primary porosity strongly influences the very early stages of the alteration process (Casella et al., 2018; Greiner et al., 2018).

(ii) The amount, fabric, distribution and composition of the organic matter within the hard tissue define the characteristics of the secondary porosity network that results from biopolymer degradation during the first step of the hydrothermal alteration process. This secondary porosity network adds to the primary porosity and provides new pathways for the infiltration and circulation of the hydrothermal fluid within the biomaterial (Jonas et al., 2017; Casella et al., 2018). The tortuosity and permeability of this network, which depend on the shape, size and interconnectivity of its constituting pores (Forjanes et al., 2020a) define the extent of hydrothermal fluid infiltration through the hard tissue (Casella et al., 2018).

(iii) Microstructures in biological hard tissues result from an intimate interlinkage between minerals and organic matter, at all scale levels. This interlinkage determines that the architecture of the mineral component can influence the kinetics of the degradation of the organics and, thereby, modulate the formation of the secondary porosity network. Mineral microarchitecture and biopolymer characteristics are taxon or even species-specific (Carter and Clark, 1985). This explains that different biological aragonitic hard tissues show different susceptibilities to hydrothermal alteration such that, while exposed to identical hydrothermal alteration conditions, some undergo a complete overprint of their pristine features, while others remain virtually unaltered (this study and Casella et al., 2018).

(iv) The solubility of the bioaragonite depends on factors such as crystal morphology, composition and amount of occluded biopolymers. Biogenic aragonite can incorporate small amounts of Sr^{2+}, Ba^{2+} and other ionic impurities into the crystal lattice. The presence of these impurities stresses the aragonite crystal structure and the resulting effect is an increase of aragonite solubility (Lippmann 1977, 1980, 1991; Plummer and Busenberg, 1987; Astilleros et al., 2003; Prieto 2009). Alike, the occlusion of biopolymer fibrils within biogenic aragonite crystals causes anisotropic lattice distortions of their lattice (Pokroy et al., 2006). This results as well in an increased solubility of biogenic aragonite, relative to that of the non-biogenic equivalent (Chave et al., 1982; Busenberg and Plummer, 1985).

(v)   The third step that marks the progress of the alteration of aragonitic hard tissues involves the dissolution of biogenic aragonite and the precipitation of non-biogenic aragonite. Consequently, the fourth step is given by the dissolution of both aragonite types, biogenic and non-biogenic, and the concomitant precipitation of abiogenic calcite. Small differences in aragonite solubility influence the development of the dissolution-crystallization reactions and affect the kinetics of the entire alteration process and mechanism.

It should be noted that, in the presence of fluids, porosity networks have a transient nature (Putnis, 2015). The dissolution-crystallization reactions that take place during the third and fourth steps of the hydrothermal alteration process are connected to solubility and molar volume changes. When, as a result of these changes, a partial or total obliteration of the biological hard tissue porosity network takes place in the course of the third alteration step, the fourth step of the alteration process cannot progress; it is either hindered or even totally precluded (Putnis et al., 2005; Jonas et al., 2014; Putnis, 2015).

4.3 The Role of Temperature and Time in the Hydrothermal Alteration of Aragonitic Hard Tissues.

Fig. 10 summarizes the different steps of the hydrothermal alteration process experienced by the outer and inner granular shell layers of the bivalve *Arctica islandica*, the outer prismatic and inner nacreous layers of the shell of the gastropod *Haliotis ovina* and the acicular, spherulitic, skeleton of the coral *Porites* sp. when being exposed to a burial fluid at (i) 175ºC for 35 days (Casella et al., 2018; high-temperature/short-term alteration) and at (ii) 80ºC for 6 months (this study; low-temperature/long-term alteration). It is quite evident that, at both temperatures, the different hard tissues reach different stages of hydrothermal alteration.

4.3.1 High Temperature – Short Term Experiments (Work of Casella et al., 2018)

At 175ºC, the shell of *Arctica islandica* undergoes severe overprint with complete, in the outer layer, to extensive, in the inner layer, replacement of the biogenic aragonite by abiogenic calcite. Significant overprint also affects the prismatic shell layer of *Haliotis ovina*, which is extensively replaced by calcite. In contrast, the microstructures of the skeleton of *Porites* sp. and the nacreous layer of *Haliotis ovina* shells are very resistant to hydrothermal overprint. Despite being resistant to alteration, *Haliotis ovina* and *Porites* sp. show extensive formation of abiogenic aragonite. This leads to the amalgamation of aragonite acicles and fibrils, in the *Porites* sp. skeleton, and of aragonite tablets, in the nacreous portion of the *Haliotis ovina* shell. Nonetheless, the amount of biogenic aragonite replaced by abiogenic calcite is little in *Porites* sp. and negligible in *Haliotis ovina* nacre tablets. The variability of the alteration kinetics of the above mentioned hard tissues at 175 ºC was interpreted by Casella et al., (2018) as arising from the combined effect of (i) the topological characteristics of the porosity network formed as a consequence of biopolymer degradation (the first two steps of the alteration process) and (ii) the changes of the

microstructure of the biomaterial triggered by the porosity during the precipitation of new, abiogenic, aragonite (the third step of the alteration process).

At temperatures above 160 ºC, and in the presence of a hydrothermal fluid, biopolymers degrade rapidly, often within few days (Benezeth et al., 1997; Jonas et al., 2017). In the outer and inner shell layers of *Arctica islandica* and in the prismatic layer of the *Haliotis ovina* shell, aragonitic mineral units are immersed into a network of biopolymer fibrils (Casella et al., 2018). The degradation of these fibrils results in a porosity network that is pervasive, consisting of large, interconnected pores, and provides a pathway for the infiltration of the hydrothermal fluid. However, pore space is significantly reduced as new aragonite precipitates during the third step of the hydrothermal alteration process (Ritter et al., 2017; Casella et al., 2018; Pederson et al., 2019a, 2019b, 2020). The topological characteristics of this porosity network affect the replacement of the aragonitic biological hard tissue by new, abiogenic, calcite, as increased aragonite surface becomes exposed to the hydrothermal fluid. This leads to the significant overprint of the pristine features of granular *Arctica islandica* and prismatic aragonite in *Haliotis ovina* hard tissues.

The behaviour of *Porites* sp. acicular and *Haliotis ovina* nacreous aragonite against hydrothermal alteration is different. The skeleton of the coral *Porites* sp. has a vast primary porosity (Griesshaber et al., 2017; Casella et al., 2018). However, the microstructure of this biological hard tissue is very dense and compact. Accordingly, little porosity is generated within the bioaragonite as a result of biopolymer degradation. In addition, the scarce, newly formed, porosity disappears as aragonite fibres abut with each other during the third step of hydrothermal alteration process (Casella et al., 2018). This reduces the surface area of the bioaragonite that is in contact with the hydrothermal fluid. In the nacreous shell layer of *Haliotis ovina* the degradation of organic sheaths around aragonite tablets generates a large porosity network. This porosity disappears during the third hydrothermal alteration step due to abiogenic aragonite precipitation between the tablets at the sites formerly occupied by the organics. The resulting effect is extensive tablet amalgamation. Thus, in *Porites* sp. and *Haliotis ovina* nacre tablets, abiogenic aragonite formation prevents the alteration to progress further and limits the overprint of the pristine features of the hard tissue.

The Arrhenius equation predicts double reaction rate constants as temperature increases by 10ºC (Arrhenius, 1889). Accordingly, the temperature-dependent alteration processes should progress 20 times slower at 80ºC than at 175ºC. The more sluggish kinetics of the alteration process explains that, despite the longer duration (180 days) of the experiments conducted at 80ºC, all investigated hard tissues undergo a much milder overprinting of their pristine features, relative to what is observed in short-time experiments conducted at higher temperatures (e.g. Pederson et al., 2019a: (*Porites* sp. at 130ºC altered for 8 weeks and at 160ºC altered for 4 weeks; Jonas et al., 2017: *Porites* sp. and *Arctica islandica* altered at 200ºC between 1 and 20 days).

535   Biopolymer degradation, which defines the first step of the hydrothermal alteration process and generates the secondary porosity network, is, indeed, a temperature-dependent process (Moussout et al., 2016). Biopolymers decompose through processes that involve depolymerization, bond scission, loss of functional groups and formation of free radicals (Gaffey 1988; Gaffey et al., 1991). Under dry conditions, these processes take place very slowly up to temperatures that depend on the composition and the structure of the biopolymer. Biopolymer decomposition temperatures can be as high at 250ºC for small

540   biomolecules with simpler structures or might even be well above 300ºC for larger and more complex biomolecules (Tiwari and Raj, 2015). In the presence of water, biopolymer degradation accelerates significantly (Gaffey 1988; Gaffey et al., 1991; Bénézeth et al., 1997) and can reach completion, when heated for 10^4-10^5 years, even at temperatures as low as 40°C-80°C; the temperatures that prevail in the shallow burial diagenetic realm (Gaffey et al., 1991; Petrova et al., 2002; Le Bayon et al., 2011).

545

The organic component of biological hard tissues consists of complex mixtures of polysaccharides, proteins, glycoproteins and glycosaminoglycans and these degrade at different temperatures and rates (Gaffey, 1988; Gaffey et al., 1991; Tiwari and Raj, 2015) and are species-specific (Marie et al., 2011; Drake et al., 2013; Le Pabic et al., 2017). Accordingly, there will be slightly different degradation pathways for the organic matter of the hard tissues of the different organisms (Keenan and Engel,

550   2017). In addition, water-soluble and -insoluble macromolecules are found in the structural materials of biocarbonates (Weiner and Traub, 1984; Goffredo et al., 2011; Sancho-Tomás et al., 2013). Therefore, it is likely that, prior to the complete degradation of the biopolymers, the organic matrices will reorganize and some of their soluble components will be released into the alteration fluid, especially at low temperatures. Since biopolymers contain a variety of functional groups, this release can influence the progress of the hydrothermal alteration. It is well known that active moieties like peptide or carboxylic groups

555   affect both the dissolution and the crystallization of calcium carbonate polymorphs through a variety of mechanisms. This influence is especially important when, as it occurs in the experiments conducted in this study, the fluid phase contains Mg^{2+} ions, as the latter inhibit the crystallization of calcite and promote the formation of the less stable aragonite (Berner 1975; Fernández-Díaz et al., 1996; Morse et al., 2007, De Choudens-Sanchez and González, 2009; Astilleros et al., 2010; Nielsen et al., 2013; Sun et al., 2015). It has been reported that the inhibitory effect of Mg^{2+} ions for calcite crystallization can be overcome

560   with hydrophilic peptides since they enhance Mg^{2+} desolvation and shift the $CaCO_3$ polymorphic distribution towards the formation of Mg-calcite (Stephenson et al., 2008; Wang et al., 2009; Nindiyasari et al., 2014a; 2014b; Yin et al., 2019). Similar Mg-calcite crystallization-promoting effects have been observed in $CaCO_3$ crystallization experiments conducted in the presence of proteinaceous extracts from a variety of coral skeletons (Sancho-Tomás et al., 2013, 2016).
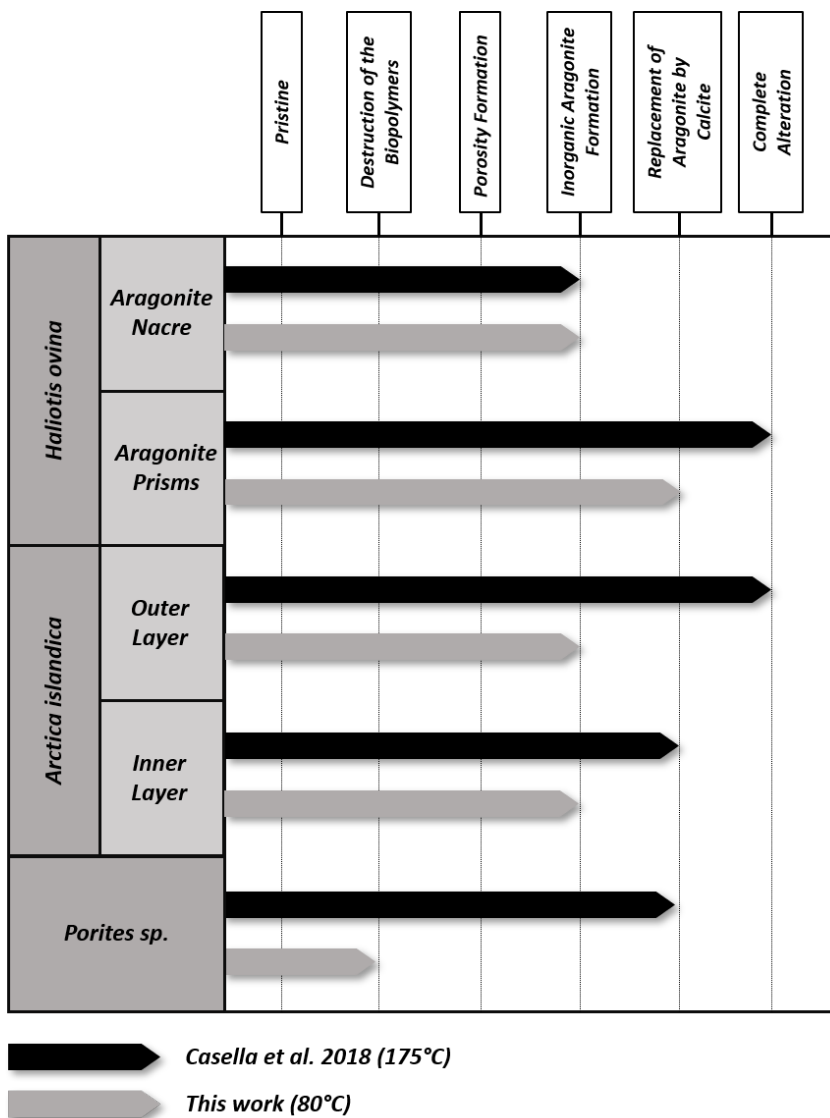
Figure 10. Main intermediate stages of alteration reached by the different aragonitic microstructures from this work when hydrothermally altered at 80ºC (this work) and 175ºC (Casella et al., 2018). In general, alteration at higher temperatures alter the microstructures more, so they reach further alteration stages. Contrarily, when the temperature is lower, the alteration is milder and the aragonitic microstructures reach previous alteration stages.

4.3.2 Long Temperature, Long Term Experiments (this work)

575 The organic matrix of *Porites* sp. and *Arctica islandica* are fully decomposed only at temperatures $\geq$ 160ºC, while at 100ºC only some dissolution and redistribution of the organics is observed, even after 20 weeks of alteration (Jonas et al., 2017, Ritter et al., 2017; Pederson et al., 2019a, 2019b, 2020). In this work, with alteration taking place for even a longer time, 24 weeks, the slower kinetics of biopolymer decomposition at 80ºC explains the small loss of organics in the case of *Porites* sp. Despite the high primary porosity of coral skeletons and the high amount of soluble macromolecules in coral organic matter, the

580 smallest biopolymer loss (7 wt.%) is observed in the skeleton of *Porites* sp. This minor loss of organics is most likely a consequence of the combined effect of slow degradation kinetics coupled to the protecting effect of the very dense coral microstructure. The compactness of *Porites* sp. skeletal aragonite restricts the interaction between the organic matter and the hydrothermal fluid to the outer surfaces of the skeleton and to the calcification centres. Hence, significant biopolymer dissolution and remobilization within coral aragonite is hindered.

585

In contrast, significant decomposition of organics is found in the altered shells of *Haliotis ovina*. (20 wt.%) and *Arctica islandica*. (30 wt.%), respectively. This high impact of the low-temperature hydrothermal conditions on the dissolution/decomposition of the organic substance is most likely a consequence of the less compact nature of the microstructures of these shells (Casella et al., 2018; Greiner et al., 2018) and is further modulated by the ratio between soluble

590 and insoluble macromolecules and spatial arrangements of the organic matrix in *Haliotis ovina* and *Arctica islandica* hard tissues.

Our study shows that the difference in dissolution/decomposition of organics present within the hard tissues is a key parameter in the generation of different volumes of secondary porosity, which adds up to the primary porosity initially present in the studied biomaterials. Accordingly, the hard tissue of *Porites* sp. shows a negligible 0.1 wt.% replacement of pristine

595 bioaragonite by abiogenic calcite at 80 °C. Pristine and altered samples of *Porites* sp. consist of aragonite crystals that are poorly co-oriented: EBSD scans show identical MUD values: 10 (Fig. 6). In addition, significant differences between the surfaces of pristine and altered *Porites* sp. samples cannot be detected. AFM images show that pristine and altered *Porites* sp. surfaces consist of similarly shaped and sized grains, without any detectable signs of mineral unit amalgamation. Statistical

600 analysis of grain size distribution yields no significant difference in grain size between pristine and altered *Porites* sp. samples. On the basis of all these observations we come to the conclusion that *Porites* sp. skeletons are extremely resistant to long-term hydrothermal alteration at low temperatures. This conclusion is in good agreement with the limited overprint experienced by *Porites* sp. skeletons in short-term hydrothermal alteration experiments, performed at significantly higher temperatures, 175 °C (Casella et al., 2018; Pederson et al., 2019a). Nevertheless, we cannot completely discard that the microstructure of *Porites*

605 sp. may have undergone some minor modifications bypassed by the analytical techniques used in this work. The skeleton of *Porites* sp. was the only one among the samples studied in this work that was collected post-mortem. Therefore, it may have

undergone some modifications prior to the beginning of the hydrothermal alteration experiments due to the metabolism of bacteria, algae, boring organisms, etc. Some signs in figure A12 hint to these modifications, which may have created additional routes for the migration of the diagenetic fluids. In any case, the extensive precipitation of abiogenic aragonite that characterizes the second step of the alteration of aragonitic hard tissues was not detected in *Porites* sp. by any of the techniques used in this work. This contrasts with the results of Casella et al., (2018) where, apart from extensive aragonite transformation into calcite, a reorganization of the aragonite crystals was observed (increase of MUD value, morphological changes in the crystals, etc.). These changes have not been observed in this work

The altered shell of *Arctica islandica* exhibits at 80 °C little replacement (1 wt. %) of aragonite by abiogenic calcite, even though, many of the original features of *Arctica islandica* shells appear to be moderately overprinted in the altered samples. Compared to pristine *Arctica islandica* shells, altered samples consist of aragonite crystals that are less co-oriented, with a drop in the MUD values from 59 to 16 in the inner layer, and from 8 to 4 in the outer layer, respectively. The drop in aragonite crystal co-orientation strength correlates with an increase in aragonite grain size. The growth in aragonite grain size is well detectable with AFM imaging (Fig. 5), where signs of crystal amalgamation are clearly visible. These changes can be explained as the result of the generation of a relatively small amount of secondary porosity, most likely due to remobilization and dissolution of soluble macromolecules. These may be released to the fluid at incipient decomposition of insoluble biopolymers. The poorly structured nature of inner and outer layers of the *Arctica islandica* shell facilitates the connection between pores in the secondary porosity network and facilitates, accordingly, the interaction with the alteration fluid.

When the hydrothermal overprint starts, the fluid is equilibrated with atmospheric CO_2 and contains no Ca^{2+}. Therefore, it is undersaturated with respect to aragonite, a disequilibrium that triggers the dissolution of the carbonate hard tissue. It was explained above that biogenic aragonites are more soluble than their abiogenic counterparts due to the anisotropic distortion caused by the occlusion of biopolymers into the aragonite structure. Therefore, once the hydrothermal fluid in the pores becomes equilibrated with the biogenic aragonite of *Arctica islandica*, it becomes supersaturated with respect to abiogenic aragonite and, more so, with respect to calcite. At this stage, the nucleation of both phases is possible in the pores (Ruiz-Agudo et al., 2014).

Two main factors might promote the formation of abiogenic aragonite instead of abiogenic calcite: (i) the presence of Mg^{2+} ions in the fluid, which inhibits the nucleation and growth of calcite (Berner 1975; Fernández-Díaz et al., 1996; Morse et al., 2007, Astilleros et al., 2010; Nielsen et al., 2013), and, therefore, promotes the precipitation of metastable aragonite and, (ii) the energy barrier associated with heterogeneous nucleation, which is reduced when the substrate and the overgrowth have the same nature (Van der Merwe 1978; Chernov, 1984; Forjanes et al., 2020b). Therefore, the epitactic growth of aragonite on the pre-existing aragonite grains is favoured over calcite. In our study, the formation of aragonite nuclei explains the increase in the average size of aragonite grains in altered samples. Since aragonite grains in pristine *Arctica islandica* shells are little co-

oriented, epitactic growth of abiogenic aragonite can also cause a reduction in MUD values of the altered samples. In addition, epitactic growth of abiogenic aragonite leads to amalgamation of aragonite crystals and destruction of porosity. Reduction of porosity and crystal amalgamation limits the percolation of the hydrothermal fluid within the hard tissue and prevents that the fourth alteration step, the replacement of aragonite by calcite, reaches any significance in any layer of *Arctica islandica* shells,

645   at least within the duration of experiments conducted in this study.

The size distribution of aragonite crystals is different between pristine and altered *Arctica islandica* shells. Large-sized crystals are more frequent while small-sized crystals are less frequent, in both, the inner and the outer layers of altered *Arctica islandica* shells, relative to those measured in the pristine hard tissue. This difference in grain size distribution can be explained by the

650   development of an Ostwald ripening process in which the preferential dissolution of the smallest, less stable, aragonite grains and the simultaneous growth of the largest crystals reduces the surface free energy of the system and results in an increase of the average aragonite crystal size and a shift of crystal size distribution towards higher values (Baronnet, 1982; Kile et al., 2000; Noguera et al., 2006; Vetter et al., 2013). Ostwald ripening processes occur under low levels of supersaturation, as it is the case for the biogenic aragonite dissolution-abiogenic aragonite precipitation reaction (Baronnet, 1982).

655

The strongest replacement of aragonite by abiogenic calcite during hydrothermal alteration at 80ºC is observed for the shell of *Haliotis ovina* (16 wt.%). However, this replacement occurs exclusively in the prismatic shell layer, while, for the experiments conducted in this study, no replacement is observable in the nacreous shell layer of *Haliotis ovina*. Other hydrothermal alteration characteristics are also developed differently in the two shell layers of *Haliotis ovina*. While aragonite crystals in the

660   prismatic shell layer become smaller-sized and less co-oriented, with a drop from 19 to 8 in MUD value, in the nacreous layer the size and the co-orientation strength of aragonite crystals increase significantly with progressive overprint. The very different response of *Haliotis ovina* prismatic and nacreous layers to hydrothermal alteration is a consequence of their different microstructures as well as content and distribution of biopolymers. Nacre is the aragonitic microstructure with the highest content of biopolymers of the samples investigated in this study (Fig. 5). AFM imaging of the altered nacreous shell layer

665   depicts the formation of grooves between the nacre tablets. This is indicative of an extensive dissolution/decomposition of the organic sheaths that envelope the tablets and results in the generation of a large volume of interconnected secondary porosity. This porosity facilitates the infiltration of the nacreous layer by the hydrothermal fluid.

The decay of biopolymers also generates a certain volume of secondary porosity in the prismatic shell layer. The less structured

670   microstructure of this layer might induce that this porosity has also a high interconnectivity, even if its volume is smaller, relative to that of the nacreous shell layer. In both layers, secondary porosity guarantees the interaction with the hydrothermal fluid over an enlarged surface of the mineralized tissue. During the first 4 months of hydrothermal alteration there is no significant replacement of aragonite by calcite (Fig. A2). Therefore, it can be assumed that once the hydrothermal fluid equilibrates locally with the biogenic aragonite in the pores and becomes supersaturated with respect to abiogenic aragonite,

675 aragonite nucleation will take place. Aragonite nucleation triggers the dissolution of biogenic aragonite and the crystallization of abiogenic aragonite through the formation of a dissolution-crystallization crystallization loops. (Putnis, 2002, 2009; Ruiz-Agudo et al., 2014). The evolution in crystal size distribution in the prismatic and the nacreous layers in *Haliotis ovina* indicates that this feedback affects both shell layers, however, in a different way. Whereas the crystal size of the prismatic aragonite decreases during progressive alteration; the opposite occurs in the nacreous layer, where crystal size increases. The difference

680 in aragonite crystal size evolution can be explained if most biogenic aragonite dissolution takes place in the prismatic layer and most abiogenic aragonite growth occurs in the nacreous layer. This interpretation is supported by the clear signs of nacre tablet amalgamation that is observed in AFM images of the altered nacreous shell layer (Fig. 4 and 5). A preferential epitactic nucleation and subsequent growth of abiogenic aragonite on nacre tablets explains the large increase in aragonite co-orientation strength in the nacreous layer during hydrothermal alteration at 80ºC. Several factors can favour abiogenic aragonite nucleation

685 on nacre tables rather than on the aragonite prisms. Not all crystal surfaces are equally stable and the fibre-shaped crystals in the prismatic layer may be more prone to dissolution, relative to nacre tablets. Differences in the amount of biopolymer fibrils occluded in each type of crystals may also affect they relative stability. The epitactic growth of abiogenic aragonite on nacre tablets and the subsequent tablet amalgamation eliminates all the secondary porosity, making it very resistant to further hydrothermal alteration. Once nacre tablets growth is no longer possible, abiogenic calcite eventually nucleates within the

690 prismatic layer. This nucleation triggers the aragonite dissolution-calcite crystallization reaction, whose development, even though limited for the timespan of the performed experiments in this study, may have contributed to further decrease of the size of the aragonite crystals in the prismatic layer of the altered *Haliotis ovina* shell.

5 Conclusions

695

The susceptibility of biocarbonates to resist diagenetic overprint is strongly influenced by several primary features, such as the carbonate phase, the microstructure of the mineral component or the distribution and fabric of the organic matter within the composite hard tissue, among others. Laboratory-based hydrothermal alteration experiments offer important insights into the fate of biocarbonate hard tissues when responding to diagenetic alteration. While previous studies investigated the effect of

700 high-temperature and short-term hydrothermal alteration on the change of biocarbonate microstructures (Casella et al., 2017, Casella et al., 2018, Pederson et al., 2019a, 2019b, 2020), the emphasis of this work is placed on the influence of low-temperature and long-term hydrothermal overprint processes of biologically secreted aragonite microstructures.

We deduce from our study the following conclusions:

705

1. We identify several intermediate stages during the overprint of aragonitic hard tissues: (I) decomposition of biopolymers, (II) gain of secondary porosity, (III) dissolution of the biogenic aragonite and precipitation of abiogenic aragonite, (IV) replacement of the biogenic and abiogenic aragonite by abiogenic calcite.

2. Depending on the composition, fabric and pattern of distribution of the organic matter within the biological hard tissue, hydrothermal alteration induces the formation of secondary porosity. The latter porosity adds to the primary porosity and facilitates the penetration and circulation of the hydrothermal fluid.

3. The porosity network greatly affects the kinetics of the alteration process, irrespective of the alteration temperature. The tortuosity and permeability of the porosity network defines the extent of infiltration and percolation of the alteration fluid into the hard tissue. This explains that different biological aragonitic hard tissues show different susceptibilities to hydrothermal alteration. For similar alteration conditions, some microstructures undergo significant to complete overprint of their pristine features, while others remain virtually unaffected.

4. For most aragonitic microstructures, except for the microstructure of *Porites* sp., incipient formation of abiogenic aragonite is observed at the very beginning of the overprint process. Biogenic aragonite dissolves and recrystallizes into abiogenic aragonite.

5. Precipitation of abiogenic aragonite occurs always prior to calcite precipitation. This is supported by the observation of several processes affecting the aragonitic microstructures which take place without a phase change. These processes are: the increase in the size of the aragonite crystals, the amalgamation of adjacent crystals and the decrease in crystal co-orientation strength for amalgamated crystals.

6. Our results have major implications for paleoenvironmental reconstruction based on proxy data gained from fossil archives. Our findings suggest that, due to diagenesis, most fossil carbonate hard tissues are overprinted, even if they do not show clear signs of carbonate phase change and microstructure destruction.

Author contributions. PF, EG, LFD and WWS designed the study. NL provided sample material. PF performed the experiments. PF, MG, MSR, SVV conducted the analyses and carried out the evaluation and merging of data. PF, EG, JMA, LFD and drafted the manuscript. All authors contributed to discussions and the final manuscript.

Competing interests. The authors declare that they have no conflict of interest.

Acknowledgements. This study was supported by the MINECO (Spain) under project CGL2016-77138-C2-1-P. PF acknowledges a FPU predoctoral contract (FPU17/01689) from the Spanish Ministry of Universities. We acknowledge the European Union's Horizon 2020 Research and Innovation Program (Grant Agreement 643084) and the German Research Council Program (GR 9/1234)

6 References

745

Arrhenius, S.: Über die Reaktionsgeschwindigkeit bei der Inversion von Rohrzucker durch Säuren. Z. Phys. Chem., 4, 226-248, 1889.

Astilleros, J.M., Pina, C.M., Fernández-Diaz, L. and Putnis, A.: Metastable phenomena on calcite {1014} surfaces growing

750   from Sr^{2+}– Ca^{2+}– CO_3^{2-} aqueous solutions. Chem. Geol., 193, 93-107, 2003.

Astilleros, J.M., Fernández-Díaz, L. and Putnis, A.: The role of magnesium in the growth of calcite: An AFM study. Chem. Geol., 271, 52-58, 2010.

755   Baronnet A.: Ostwald ripening: The case of calcite and mica. Estud. Geol., 38, 185–198, 1982

Bénézeth, P., Palmer, D. A., and Wesolowski, D. J.: Dissociation quotients for citric acid in aqueous sodium chloride media to 150 C. J. Solut. Chem., 26, 63-84, 1997.

760   Bernard, S., Daval, D., Ackerer, P., Pont, S. and Meibom, A. Burial-induced oxygen-isotope re-equilibration of fossil foraminifera explains ocean paleotemperature paradoxes. Nat. Commun., 8, 1-10. 2017.

Berner, R. A.: The role of magnesium in the crystal growth of calcite and aragonite from sea water, Geochim. Cosmochim. Ac., 39, 489–504, 1975.

765

Bischoff, J. L.: Kinetics of calcite nucleation: magnesium ion inhibition and ionic strength catalysis, J. Geophys. Res., 73, 3315–3322, 1968.

Bischoff, J. L.: Temperature controls on aragonite-calcite transformation in aqueous solution, Am. Mineral., 54, 149–155,

770   1969.

Bischoff, W. D., Mackenzie, F. T., and Bishop, F. C.: Stabilities of synthetic magnesian calcites in aqueous solution: Comparison with biogenic materials. Geochim. Cosmochim. Ac., 51, 1413-1423, 1987.

775   Bischoff, W. D., Bertram, M. A., Mackenzie, F. T., and Bishop, F. C.: Diagenetic stabilization pathways of magnesian calcites. Carbonates Evaporites, 8, 82-89, 1993.

Busenberg, E. and Plummer, L.N.: Kinetic and thermodynamic factors controlling the distribution of SO_4^{2-} and Na^+ in calcites and selected aragonites. Geochim. Cosmochim. Ac., 49, 713-725. 1985.

Brand, U.: Biogeochemistry of Late Palaeozoic North American brachiopods and secular variation of seawater composition. Biogeochemistry, 7, 159-193, 1989.

Cardew, P.T. and Davey, R.J.: The kinetics of solvent-mediated phase transformations. Proc. R. Soc. A., 398, 415-428, 1985.

Carter, J. G., and Clark, G. R.: Classification and phylogenetic significance of molluscan shell microstructure. Studies in Geology, Notes for a Short Course, 13, 50-71, 1985.

Casella, L.A., Griesshaber, E., Yin, X., Ziegler, A., Mavromatis, V., Müller, D., Ritter, A.C., Hippler, D., Harper, E.M., Dietzel, M. and Immenhauser, A.: Experimental diagenesis: insights into aragonite to calcite transformation of *Arctica islandica* shells by hydrothermal treatment. Biogeosciences, 14, 1461-1492, 2017.

Casella, L.A., He, S., Griesshaber, E., Fernández-Díaz, L., Greiner, M., Harper, E.M., Jackson, D.J., Ziegler, A., Mavromatis, V., Dietzel, M. and Eisenhauer, A.: Hydrothermal alteration of aragonitic biocarbonates: assessment of micro-and nanostructural dissolution–reprecipitation and constraints of diagenetic overprint from quantitative statistical grain-area analysis. Biogeosciences, 15, 7451-7484, 2018.

Chave, K. E., Deffeyes, K. S., Weyl, P. K., Garrels, R. M., and Thompson, M. E.: Observations on the solubility of skeletal carbonates in aqueous solutions. Science, 137, 33-34, 1982.

Cisneros-Lazaro, D., Adams, A., Guo, J., Bernard, S., Daval, D., Baronnet, A., Grauby, O., Vennemann, T., Stolarski, J., Baumgartner, L. and Meibom, A. Species-specific foraminiferal ultrastructures modulate surfaces available for diagenesis. Microsc. Microanal., 27, 274-275, 2021.

Cisneros-Lazaro, D., Adams, A., Guo, J., Bernard, S., Baumgartner, L.P., Daval, D., Baronnet, A., Grauby, O., Vennemann, T., Stolarski, J. and Escrig, S. Fast and pervasive diagenetic isotope exchange in foraminifera tests is species-dependent. Nat. Commun., 13, 1-11, 2022.

Chernov, A. A.: Nucleation and epitaxy. In Modern Crystallography III, 48-103, 1984.

810   Cherns, L., Wheeley, J.R. and Wright, V.P.: Taphonomic bias in shelly faunas through time: early aragonitic dissolution and its implications for the fossil record. In Taphonomy, 79-105, 2011.

Cherns, L. and Wright, V. P.: Skeletal mineralogy and biodiversity of marine invertebrates: size matters more than seawater chemistry. Geological Society, London, Special Publications, 358, 9-17, 2011

815

De Choudens-Sanchez, V. and Gonzalez, L.A.: Calcite and aragonite precipitation under controlled instantaneous supersaturation: elucidating the role of $CaCO_3$ saturation state and Mg/Ca ratio on calcium carbonate polymorphism. J. Sediment. Res., 79, 363-376, 2009.

820   Drake, J. L., Mass, T., Haramaty, L., Zelzion, E., Bhattacharya, D., and Falkowski, P. G.: Proteomic analysis of skeletal organic matrix from the stony coral Stylophora pistillata. Proceedings of the National Academy of Sciences, 110, 3788-3793, 2013.

Fernandez-Diaz, L., Putnis, A., Prieto, M. and Putnis, C.V.: The role of magnesium in the crystallization of calcite and aragonite in a porous medium. J. Sediment. Res., 66, 482-491, 1996.

825

Forjanes, P., Astilleros, J. M., and Fernández-Díaz, L.: The formation of barite and celestite through the replacement of gypsum. Minerals, 10, 189, 2020a.

Forjanes, P., Gómez-Barreiro, J., Morales, J., Astilleros, J. M., and Fernández-Díaz, L.: Epitactic growth of celestite on
830   anhydrite: substrate induced twinning and morphological evolution of aggregates. CrystEngComm, 22, 5743-5759, 2020b.

Fyfe, W. S. and Bischoff, J. L.: The calcite-aragonite problem, Soc. Econ. Pa., 13, 3–13, 1965.

Gaffey, S.J.: Water in skeletal carbonates. J. Sediment. Res. 58, 397–414, 1988.

835

Gaffey, S.J., Kolak, J.J., and Bronnimann, C.E.: Effects of drying, heating, annealing, and roasting on carbonate skeletal material, with geochemical and diagenetic implications. Geochim. Cosmochim. Ac., 55, 1627–1640, 1991.

Gebauer, D. and Cölfen, H.: Prenucleation clusters and nonclassical nucleation, Nano Today, 6, 564–584, 2011.

840

Gebauer, D., Völkel, A., and Cölfen, H.: Stable prenucleation calcium carbonate Clusters, Science, 322, 1819–1822, 2008.

Goffredo, S., Vergni, P., Reggi, M., Caroselli, E., Sparla, F., Levy, O., Dubinsky, Z. and Falini, G.: The skeletal organic matrix from Mediterranean coral Balanophyllia europaea influences calcium carbonate precipitation. PLoS One, 6, 22338, 2011.

845

Greiner, M.; Fernández-Díaz, L.; Griesshaber, E.; Zenkert, M.N.; Yin, X.; Ziegler, A.; Veintemillas-Verdaguer, S.; Schmahl, W.W.: Biomineral Reactivity: The Kinetics of the Replacement Reaction of Biological Aragonite to Apatite. Minerals, 8, 315, 2018.

850   Griesshaber, E., Schmahl, W. W., Ubhi, H. S., Huber, J., Nindiyasari, F., Maier, B., and Ziegler, A.: Homoepitaxial meso-and microscale crystal co-orientation and organic matrix network structure in Mytilus edulis nacre and calcite. Acta Biomater., 9, 9492-9502, 2013.

Griesshaber, E., Yin, X., Ziegler, A., Kelm, K., Checa, A., Eisenhauer, A., and Schmahl, W. W.: Patterns of mineral
855   organization in carbonate biological hard materials. In Highlights in applied mineralogy, 245-272, 2017.

Hall, A., Kennedy, W. J., and Taylor, J. H.: Aragonite in fossils. Proc. R. Soc. Lond. B Biol. Sc.i, 168, 377-412, 1967.

Hallam, A., and O'Hara, M.J.: Aragonitic fossils in the Lower Carboniferous of Scotland. Nature, 195, 273-274, 1962.

860

James, N. P., Bone, Y., and Kyser, T. K.: Where has all the aragonite gone? Mineralogy of Holocene neritic cool-water carbonates, southern Australia. J. Sediment. Res., 75, 454-463, 2005.

Janiszewska, K., Mazur, M., Machalski, M., and Stolarski, J.: From pristine aragonite to blocky calcite: Exceptional
865   preservation and diagenesis of cephalopod nacre in porous Cretaceous limestones, Plos one, 13, e0208598, 2018.
Jarosch, D., and Heger, G.: Neutron diffraction refinement of the crystal structure of aragonite. Tscher. Mineral. Petr. Mitt., 35, 127-131, 1986.

Jonas, L., John, T., King, H. E., Geisler, T., and Putnis, A.: The role of grain boundaries and transient porosity in rocks as fluid
870   pathways for reaction front propagation. Earth Planet. Sci. Lett., 386, 64-74, 2014.

Jonas, L., Müller, T., Dohmen, R., Immenhauser, A., and Putlitz B.: Hydrothermal replacement of biogenic and abiogenic aragonite by Mg-carbonates–Relation between textural control on effective element fluxes and resulting carbonate phase. Geochim. Cosmochim. Ac., 196, 289-306, 2017.

875

Keenan, S. W., and Engel, A. S.: Early diagenesis and recrystallization of bone. Geochim. Cosmochim. Ac., 196, 209-223, 2017.

Kile, D. E., Eberl, D. D., Hoch, A. R., and Reddy, M. M.: An assessment of calcite crystal growth mechanisms based on crystal size distributions. Geochim. Cosmochim. Ac., 64, 2937-2950, 2000.

Le Bayon, R., Brey, G. P., Ernst, W. G., and Mählmann, R. F.: Experimental kinetic study of organic matter maturation: Time and pressure effects on vitrinite reflectance at 400 C. Org. Geochem., 42, 340-355, 2011.

Le Pabic, C., Marie, A., Marie, B., Percot, A., Bonnaud-Ponticelli, L., Lopez, P. J., and Luquet, G.: First proteomic analyses of the dorsal and ventral parts of the Sepia officinalis cuttlebone. J. Proteom., 150, 63-73, 2017.

Lippmann F.: The solubility product of complex minerals, mixed crystals and three-layer clay minerals. N. Jahrb. Mineral. Abh., 130, 243-263, 1977.

Lippmann F.: Phase diagrams depicting the aqueous solubility of binary mineral systems. N. Jahrb. Mineral. Abh., 139, 1-25, 1980.

Lippmann F.: Aqueous solubility of magnesian calcites with different endmembers. Acta. Mineral. Petrogr., 32, 5-19. 1991.

Lowenstam, H.A.: Factors affecting the aragonite: calcite ratios in carbonate-secreting marine organisms. J. Geol., 62, 284-322, 1954.

Marie, B., Le Roy, N., Zanella-Cléon, I., Becchi, M., and Marin, F.: Molecular evolution of mollusc shell proteins: insights from proteomic analysis of the edible mussel Mytilus. J. Mol. Evol., 72, 531-546, 2011.

Markgraf, S. A., and Reeder, R. J.: High-temperature structure refinements of calcite and magnesite. Am. Min., 70, 590-600, 1985.

Morse, J. W., Arvidson, R. S., and Lüttge, A.: Calcium carbonate formation and dissolution, Chem. Rev., 107, 342–381, 2007.

Moussout, H., Ahlafi, H., Aazza, M., and Bourakhouadar, M.: Kinetics and mechanism of the thermal degradation of biopolymers chitin and chitosan using thermogravimetric analysis. Polymer Degradation and Stability, 130, 1-9, 2016.

Mucci, A., Canuel, R., and Zhong, S.: The solubility of calcite and aragonite in sulfate-free seawater and the seeded growth

910   kinetics and composition of the precipitates at 25 C. Chem. Geol., 74, 309-320, 1989.

Navrotsky, A.: Energetic clues to pathways to biomineralization: Precursors, clusters, and nanoparticles, P. Natl. Acad. Sci. USA., 101, 12096–12101, 2004.

915   Nielsen, L. C., De Yoreo, J. J., and DePaolo, D. J.: General model for calcite growth kinetics in the presence of impurity ions. Geochim. Cosmochim. Ac., 115, 100-114, 2013.

Nindiyasari, F., Fernández-Díaz, L., Griesshaber, E., Astilleros, J. M., Sanchez-Pastor, N., and Schmahl, W. W.: Influence of gelatin hydrogel porosity on the crystallization of $CaCO_3$, Cryst. Growth Des., 14, 1531–1542, 2014a.

920

Nindiyasari, F., Griesshaber, E., Fernandez-Diaz, L., Astilleros, J. M., Sanchez-Pastor, N., Ziegler, A., and Schmahl, W. W.: Effects of Mg and hydrogel solid content on the crystallization of calcium carbonate in biomimetic counter-diffusion systems. Cryst. Growth Des., 14, 4790-4802, 2014b.

925   Noguera, C., Fritz, B., Clément, A., and Baronnet, A.: Nucleation, growth, and ageing scenarios in closed systems I: A unified mathematical framework for precipitation, condensation and crystallization. J. Cryst. Growth., 297, 180-186, 2006.

Pederson, C.L., Weiss, L., Mavromatis, V., Rollion-Bard, C., Dietzel, M., Neuser, R. and Immenhauser, A.: Significance of fluid chemistry throughout diagenesis of aragonitic *Porites* corals–An experimental approach. Depos. Rec., 5, 592-612, 2019a.

930

Pederson, C., Mavromatis, V., Dietzel, M., Rollion-Bard, C., Nehrke, G., Jöns, N., Jochum, K.P. and Immenhauser, A.: Diagenesis of mollusc aragonite and the role of fluid reservoirs. Earth Planet. Sci. Lett., 514, 130-142, 2019b.

Pederson, C.L., Mavromatis, V., Dietzel, M., Rollion-Bard, C., Breitenbach, S.F.M., Yu, D., Nehrke, G. and Immenhauser,

935   A.: Variation in the diagenetic response of aragonite archives to hydrothermal alteration. Sediment. Geol., 406, 105716, 2020.

Perdikouri, C., Kasioptas, A., Putnis, C.V. and Putnis, A.: The effect of fluid composition on the mechanism of the aragonite to calcite transition. Mineral. Mag., 72, 111-114, 2008.

940   Perdikouri, C., Kasioptas, A., Geisler, T., Schmidt, B. C., and Putnis, A.: Experimental study of the aragonite to calcite transition in aqueous solution, Geochim. Cosmochim. Ac., 75, 6211–6224, 2011.

Perdikouri, C., Piazolo, S., Kasioptas, A., Schmidt, B. C., and Putnis, A.: Hydrothermal replacement of Aragonite by Calcite: interplay between replacement, fracturing and growth, Eur. J. Mineral., 25, 123–136, 2013.

945

Petrova, T. V., Mahlmann, R. F., Stern, W. B., and Frey, M.: Application of combustion and DTA-TGA analysis to the study of metamorphic organic matter. Schweiz Mineral Petrogr Mitt., 82, 33-53, 2002.

Plummer, L. N. and Mackenzie, F. T.: Predicting mineral solubility from rate data; application to the dissolution of magnesian

950   calcites, Am. J. Sci., 274, 61–83, 1974.

Plummer, L. N. and Busenberg, E.: The solubilities of calcite, aragonite and vaterite in CO_2-H_2O solutions between 0 and 90 ºC, and an evaluation of the aqueous model for the system $CaCO_3$- CO_2-H_2O, Geochim. Cosmochim. Ac., 46, 1011–1040, 1982.

955

Plummer, L. N., and Busenberg, E.: Thermodynamics of aragonite-strontianite solid solutions: Results from stoichiometric solubility at 25 and 76 C. Geochim. Cosmochim. Ac., 51, 1393-1411, 1987.

Pokroy, B., Fitch, A. N., Lee, P. L., Quintana, J. P., El'ad, N. C., and Zolotoyabko, E.: Anisotropic lattice distortions in the

960   mollusk-made aragonite: a widespread phenomenon. J. Struct. Biol., 153, 145-150, 2006.

Prieto, M.: Thermodynamics of solid solution-aqueous solution systems. Rev. Mineral. Geochem., 70, 47-85, 2009.

Putnis, A.: Mineral replacement reactions: from macroscopic observations to microscopic mechanisms. Mineral. Mag, 66,

965   689-708, 2002.

Putnis, A.: Mineral replacement reactions.   Rev. Mineral. Geochem., 70, 87-124, 2009.

Putnis, A.: Transient porosity resulting from fluid–mineral interaction and its consequences. Rev. Mineral. Geochem., 80, 1-

970   23, 2015.

Putnis, C. V., Tsukamoto, K., and Nishimura, Y.: Direct observations of pseudomorphism: compositional and textural evolution at a fluid-solid interface. Am. Min., 90, 1909-1912, 2005.

975   Putnis, A. and Putnis, C.V.: The mechanism of reequilibration of solids in the presence of a fluid phase. J. Solid State Chem., 180, 1783-1786, 2007.

Radha, A. V. and Navrotsky, A.: Thermodynamics of carbonates, Rev. Mineral. Geochem., 77, 73–121, 2013.

980 Radha, A. V., Forbes, T. Z., Killian, C. E., Gilbert, P. U. P. A., and Navrotsky, A.: Transformation and crystallization energetic of synthetic and biogenic amorphous calcium Carbonate, PNAS, 107, 16438–16443, 2010.

Randle, V.: Theoretical framework for electron backscatter diffraction. In Electron backscatter diffraction in materials science, 19-30, 2000.

985

Redfern, S. A. T., Salje, E., and Navrotsky, A.: High-temperature enthalpy at the orientational order-disorder transition in calcite: implications for the calcite/aragonite phase equilibrium, Contrib. Mineral. Petr., 101, 479–484, 1989.

Ritter, A.C., Mavromatis, V., Dietzel, M., Kwiecien, O., Wiethoff, F., Griesshaber, E., Casella, L.A., Schmahl, W.W., Koelen,
990 J., Neuser, R.D. and Leis, A.: Exploring the impact of diagenesis on (isotope) geochemical and microstructural alteration features in biogenic aragonite. Sedimentology, 64, 1354-1380, 2017.

Rodríguez-Carvajal, J.: FullProf. CEA/Saclay, France, 2001.

995 Ruiz-Agudo, E., Putnis, C.V. and Putnis, A.: Coupled dissolution and precipitation at mineral–fluid interfaces. Chem. Geol., 383, 132-146, 2014.

Sancho-Tomás, M., Fermani, S., Durán-Olivencia, M. A., Otálora, F., Gómez-Morales, J., Falini, G., and García-Ruiz, J. M.: Influence of charged polypeptides on nucleation and growth of $CaCO_3$ evaluated by counterdiffusion experiments. Cryst.
1000 Growth Des., 13, 3884-3891, 2013.

Sancho-Tomás, M., Fermani, S., Reggi, M., García-Ruiz, J. M., Gómez-Morales, J., and Falini, G.: Polypeptide effect on Mg^{2+} hydration inferred from $CaCO_3$ formation: a biomineralization study by counter-diffusion. CrystEngComm, 18, 3265-3272, 2016.

1005

Sandberg, P.A. and Hudson, J.D.: Aragonite relic preservation in Jurassic calcite-replaced bivalves. Sedimentology, 30, 879-892, 1983.

Sass, E., Morse, J. W., and Millero, F. J.: Dependence of the values of calcite and aragonite thermodynamic solubility products
1010 on ionic models, Am. J. Sci., 283, 218–229, 1983.

Schmidt, N. H., and Olesen, N. O.: Computer-aided determination of crystal-lattice orientation from electron channeling patterns in the SEM. Canad. Mineral., 27, 15-22, 1989.

1015 Seuß, B., Nützel, A., Mapes, R. H., and Yancey, T. E.: Facies and fauna of the Pennsylvanian Buckhorn Asphalt Quarry deposit: a review and new data on an important Palaeozoic fossil Lagerstätte with aragonite preservation. Facies, 55, 609, 2009.

Simonet Roda, M., Griesshaber, E., Ziegler, A., Rupp, U., Yin, X., Henkel, D., Häussermann, V., Laudien, J., Brand, U., 1020 Eisenhauer, A. and Checa, A.G. Calcite fibre formation in modern brachiopod shells. Sci. Rep., 9, 1-15, 2019.

Simonet Roda, M., Griesshaber, E., Angiolini, L., Rollion-Bard, C., Harper, E.M., Bitner, M.A., Milner Garcia, S., Ye, F., Henkel, D., Häussermann, V. and Eisenhauer, A. The architecture of Recent brachiopod shells: diversity of biocrystal and biopolymer assemblages in rhynchonellide, terebratulide, thecideide and craniide shells. Mar. Biol., 169, 1-52. 2022.

1025 Stephenson, A. E., DeYoreo, J. J., Wu, L., Wu, K. J., Hoyer, J., and Dove, P. M.: Peptides enhance magnesium signature in calcite: insights into origins of vital effects. Science, 322, 724-727, 2008.

Sun, W., Jayaramana, S., Chen, W., Persson, K. A., and Cedera, G.: Nucleation of metastable aragonite $CaCO_3$ in seawater, 1030 PNAS, 112, 3199–3204, 2015.

Swart, P. K.: The geochemistry of carbonate diagenesis: The past, present and future. Sedimentology, 62, 1233-1304, 2015.

Tiwari A, and Raj B.: Reactions and Mechanisms in Thermal Analysis of Advanced Materials. New York: John Wiley and 1035 Sons, 2015.

Van Der Merwe J.H.: The role of lattice misfit in epitaxy, Crit. Rev. Solid. State. Mater. Sci., 7, 209–231, 1978

Vetter, T., Igrlland, M., Ochsenbein, D. R., Hänseler, F. S., and Mazzotti, M.: Modeling nucleation, growth, and Ostwald 1040 ripening in crystallization processes: a comparison between population balance and kinetic rate equation. Cryst. Growth Des., 13, 4890-4905, 2013.

Walter, L. M., and Morse, J. W.: Reactive surface area of skeletal carbonates during dissolution; effect of grain size. J. Sediment. Res., 54, 1081-1090, 1984.

1045

Wang, D., Wallace, A. F., De Yoreo, J. J., and Dove, P. M.: Carboxylated molecules regulate magnesium content of amorphous calcium carbonates during calcification. Proc. Natl. Acad. Sci., 106, 21511-21516, 2009.

Weiner, S., and Traub, W.: Macromolecules in mollusc shells and their functions in biomineralization. Philos. Trans. R. Soc.

1050   B., 304, 425-434, 1984.

Weiner, S., and Dove, P. M.: An overview of biomineralization processes and the problem of the vital effect. Rev. Mineral. Geochem., 54, 1-29, 2003.

1055   Wright, V. P. and Cherns, L.: Are there "black holes" in carbonate deposystems? Geol. Acta, 2, 285–290, 2004.

Wright, V. P., Cherns, L., and Hodges, P.: Missing molluscs: Field testing taphonomic loss in the Mesozoic through early large scale aragonite dissolution, Geology, 31, 211–214, 2003.

1060   Yin, X., Griesshaber, E., Fernandez-Diaz, L., Ziegler, A., García-García, F. J., and Schmahl, W. W.: Influence of Gelatin– Agarose Composites and Mg on Hydrogel-Carbonate Aggregate Formation and Architecture. Cryst. Growth Des., 19, 5696- 5715, 2019.

Appendix Figures

1065
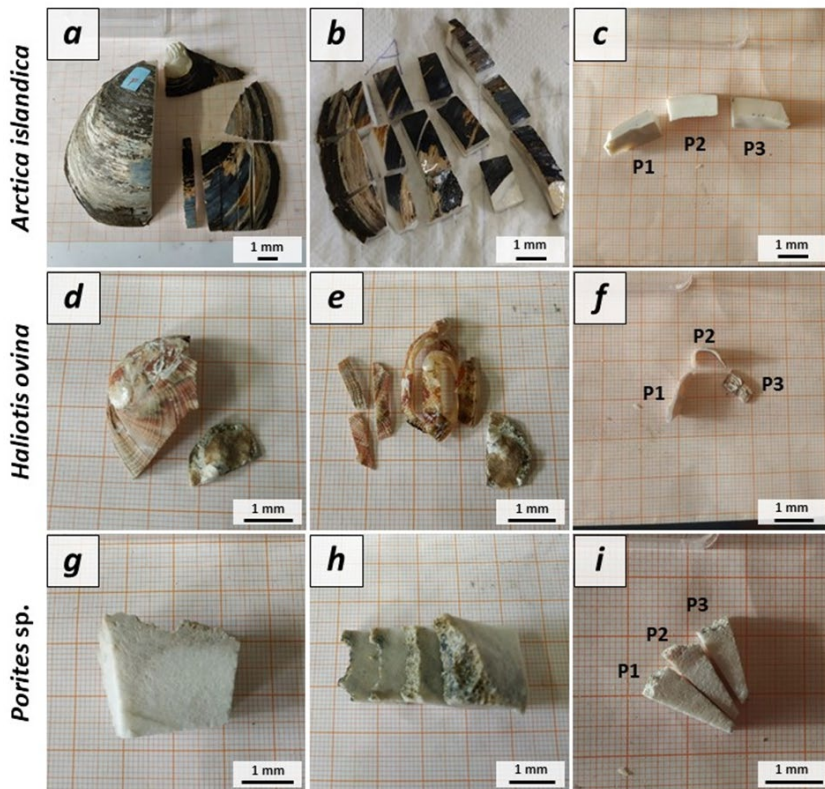
Figure A1. Preparation of *Arctica islandica*, *Haliotis ovina* shells and *Porites* sp. skeletons for hydrothermal alteration experiments. A long section was cut out of the hard tissue (Figs. A1a, d, g). Subsequently, it was sectioned into three parts: P1, P2, P3 (Figs. A1b, e, h). The pieces were then altered. P1 was used for laser confocal microscopy and atomic force microscopy (AFM) imaging; P2 was used for FE-SEM imaging and EBSD measurements and P3 was powdered and used for XRD and TGA measurements; the XRD data formed the basis for Rietveld refinements.
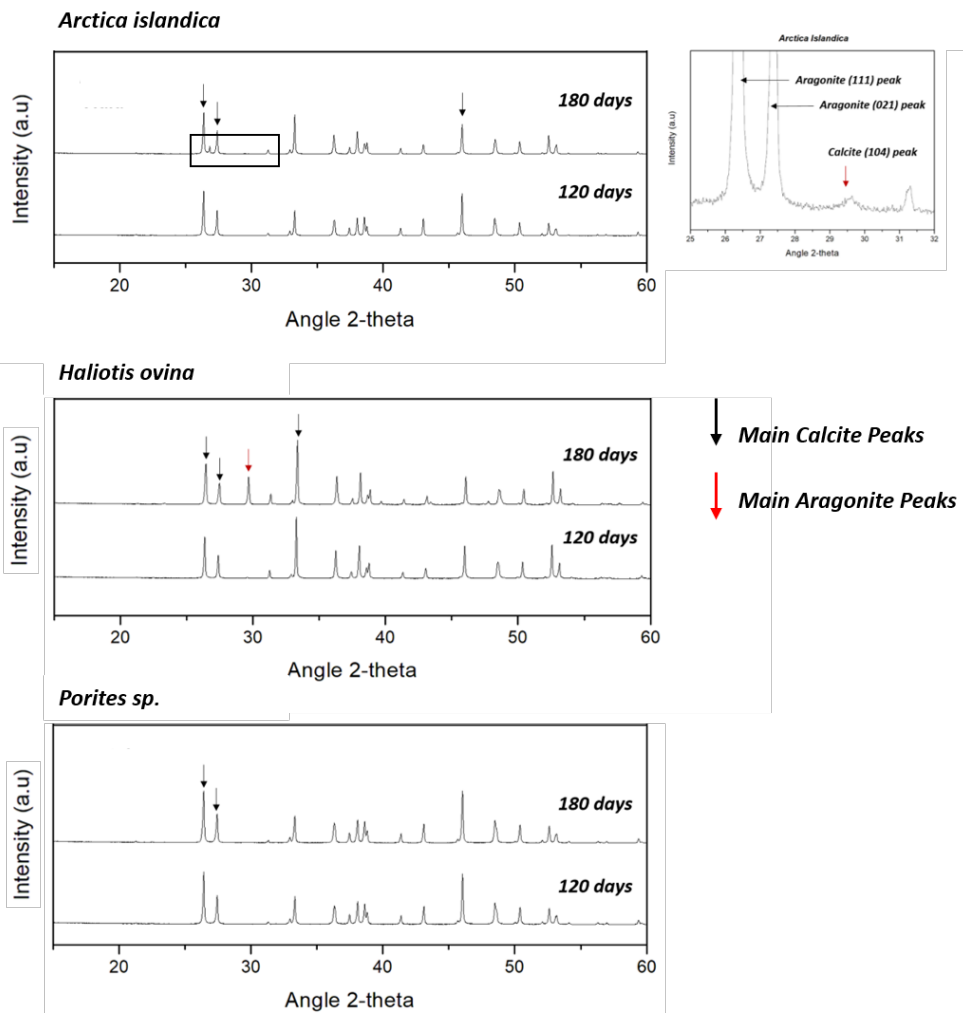
1075

Figure A2. X-ray diffractograms of the hydrothermally altered shells and skeletons of *Arctica islandica*, *Haliotis ovina* and *Porites* sp. Alteration was performed at 80°C in a Mg-rich, burial-mimicking fluid (100 mM NaCl + 10 mM MgCl₂) and lasted for 4 and 6 months.
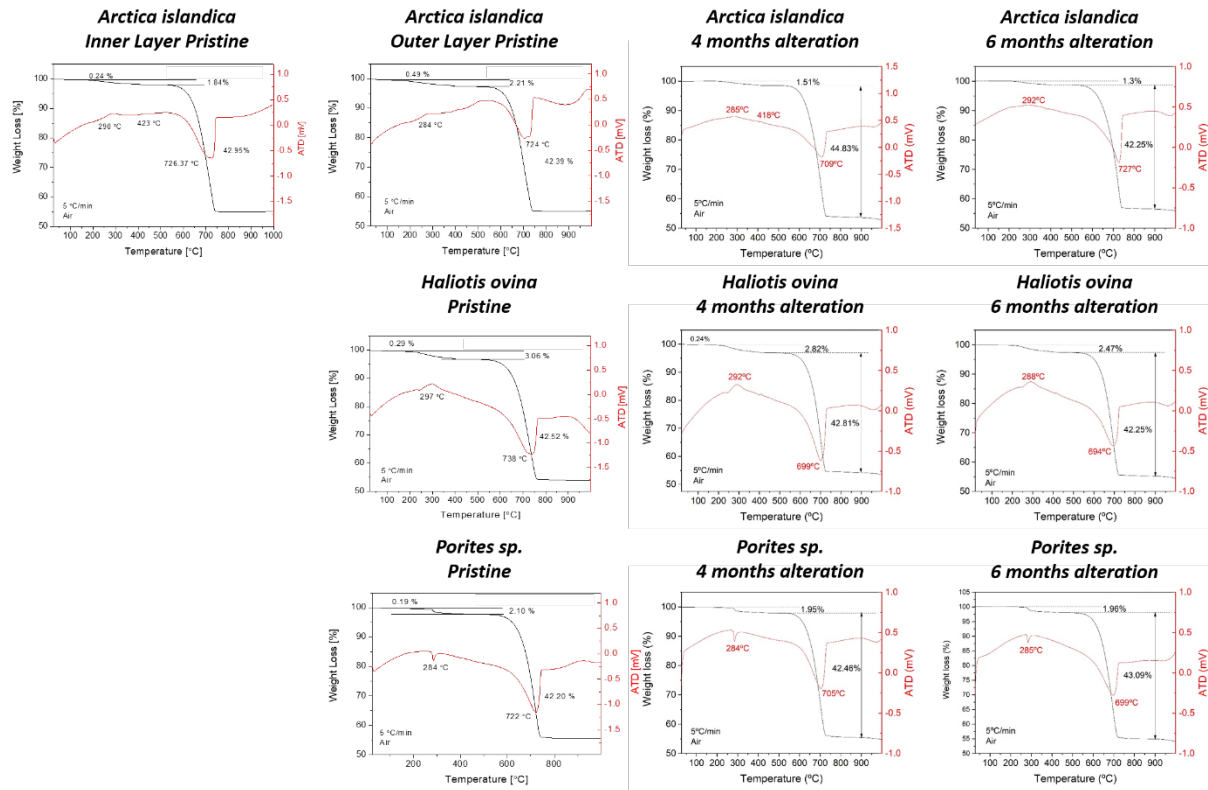
1080

Figure A3. Thermogravimetric analysis data of pristine and altered hard tissues of *Arctica islandica*, *Haliotis ovina* and *Porites* sp. shells and skeletal elements. Alteration was performed at 80°C in a Mg-rich, burial-mimicking fluid (100 mM NaCl + 10 mM MgCl₂) and lasted for 4 and 6 months.

1085

Pristine   **6 months alteration**
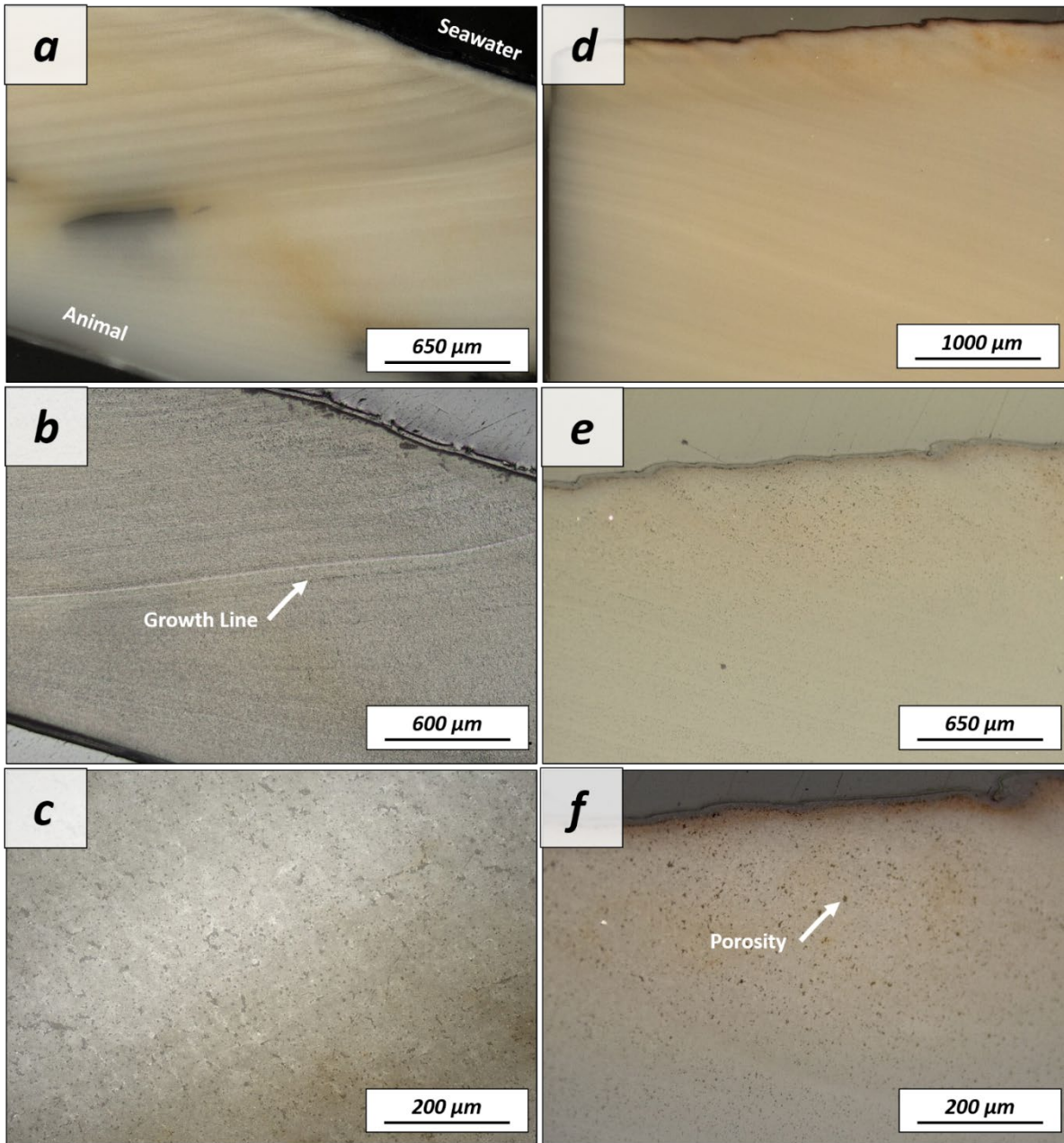
Figure A4. Laser confocal microscopy images of (a-c) pristine and (d-f) altered shells of *Arctica islandica*. The shells display a homogeneous internal structure where porosity and growth lines can be observed. After 6 months of hydrothermal alteration, major changes to the shell structure cannot be observed with laser confocal microscopy imaging.

1090
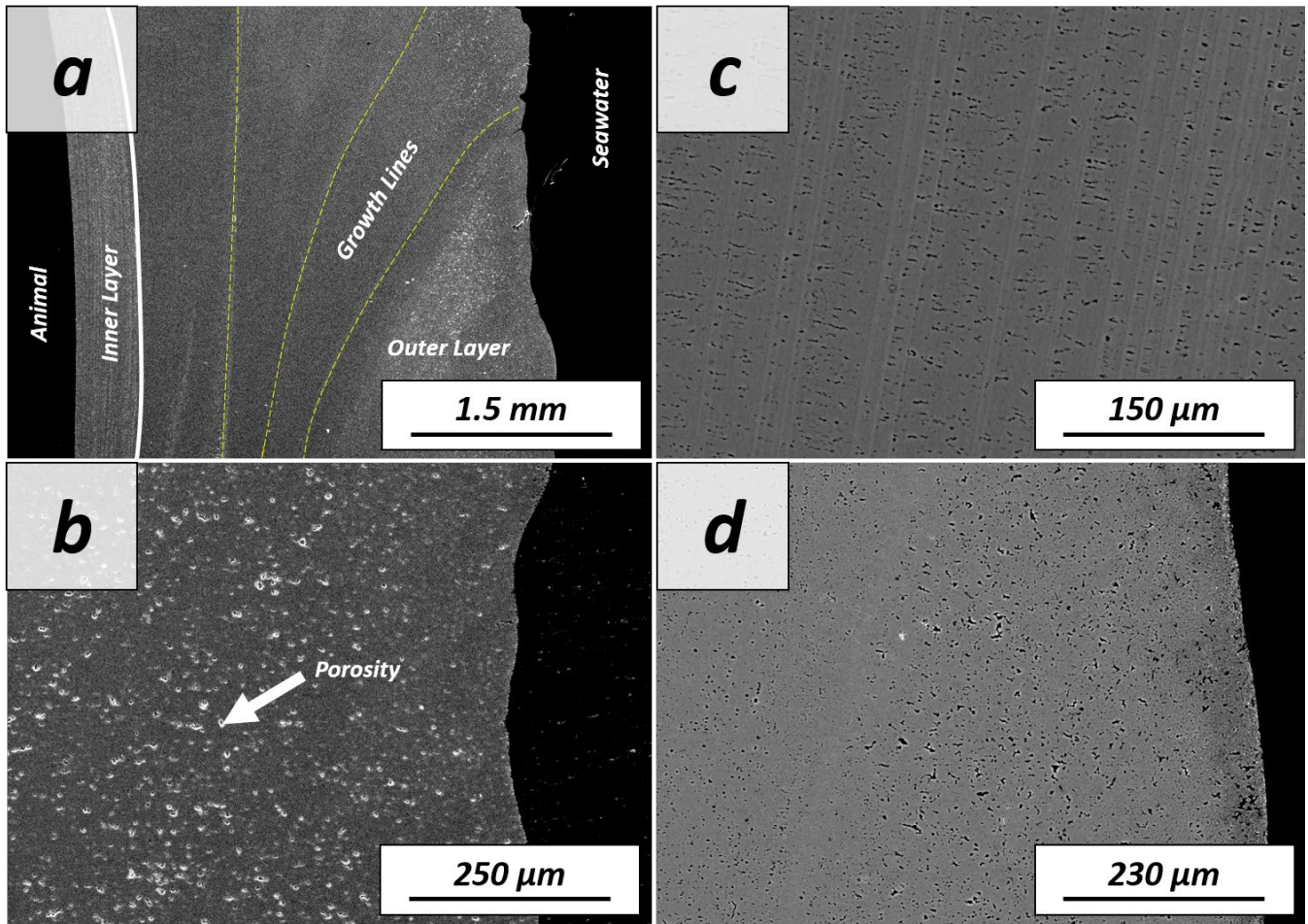
Figure A5. FE-SEM images of (a,b) pristine and (c,d) altered shells of the bivalve *Arctica islandica*. The shell consists of an assemblage of irregular aragonite crystals embedded in a network of biopolymer fibres (this study and Casella et al., 2017; 2018). Two layers comprise the shell, both with abundant pores and growth lines (c,d). Hydrothermal alteration at 80 °C in a burial-mimicking fluid, for 4 and 6 months does not inflict significant shell structure reorganization and change that can be observed with FE-SEM imaging.

1095
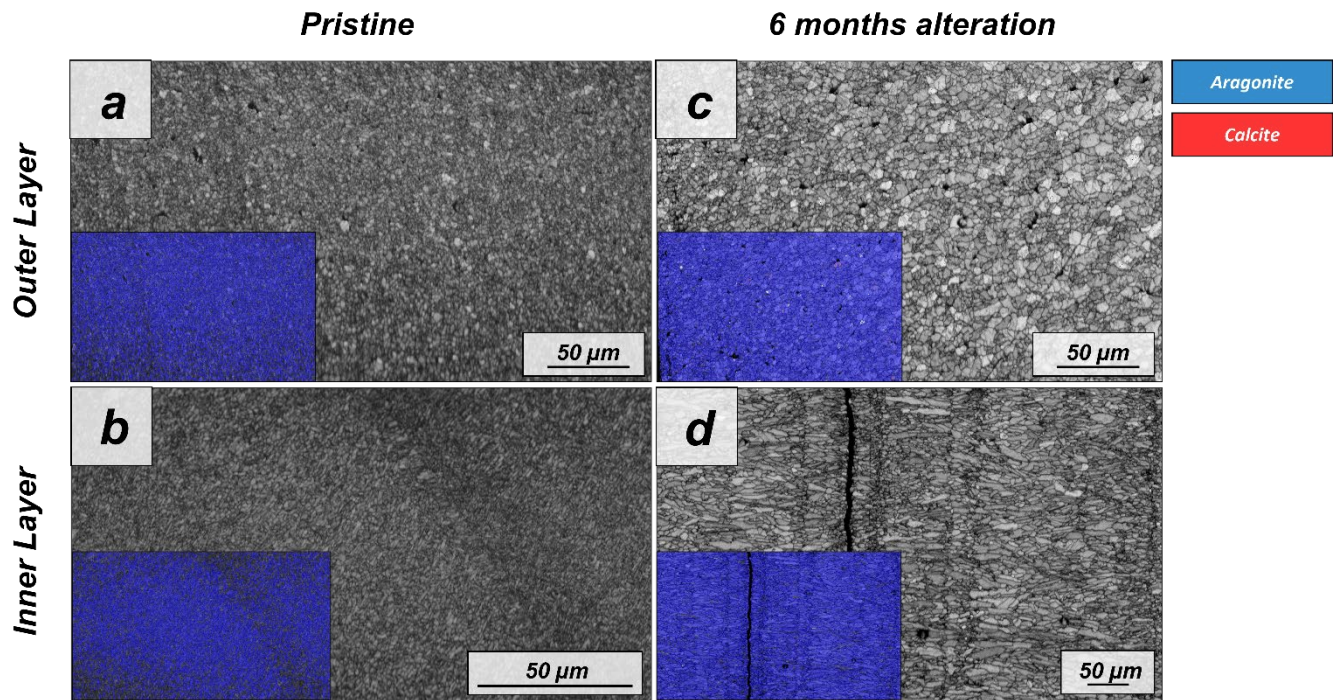
1100   **Figure A6**. EBSD band contrast and phase maps illustrating the differences in the microstructure and mineralogy between the pristine and the most altered shell of *Arctica islandica* after 6 months of hydrothermal alteration with a Mg-rich, burial, fluid at 80ºC. A phase change is not observable.

Pristine   **6 months alteration**
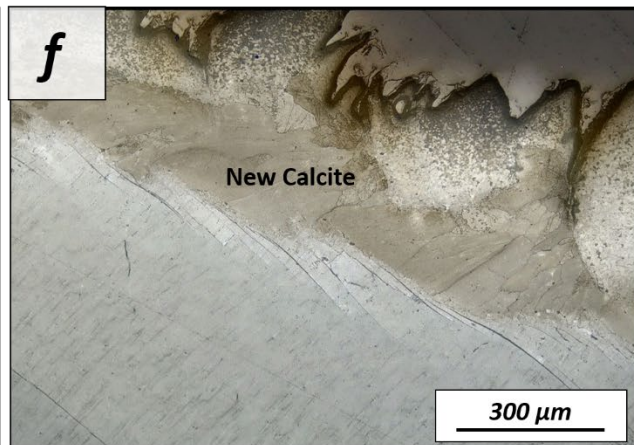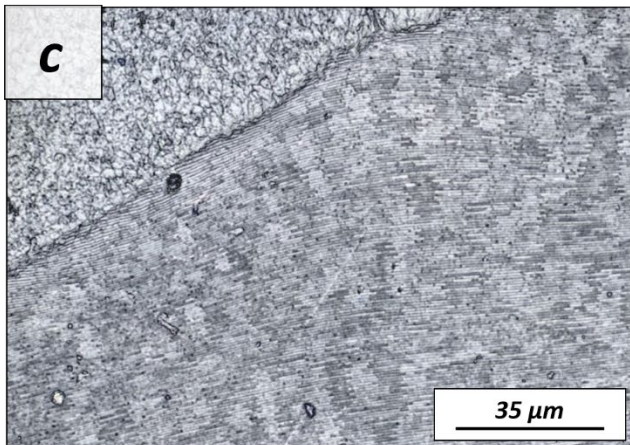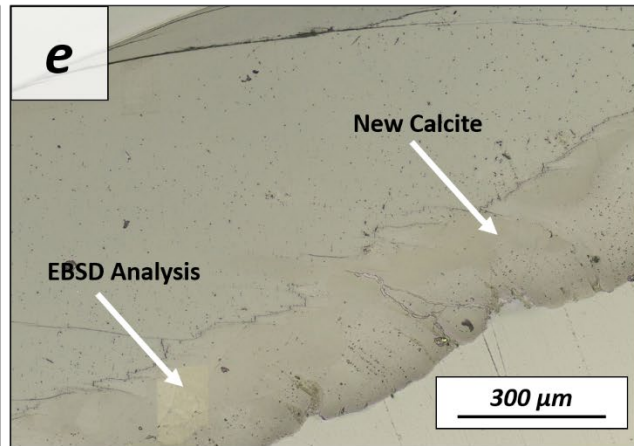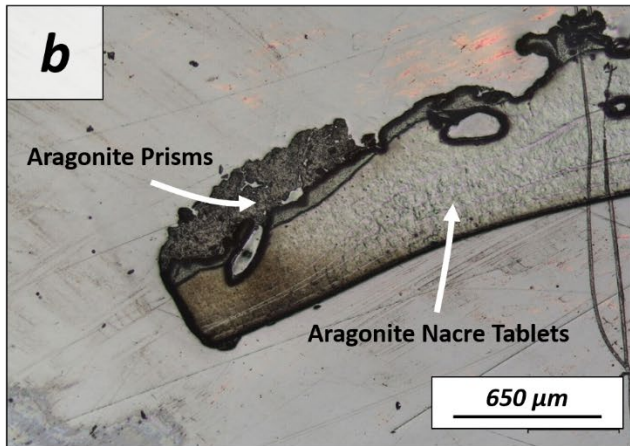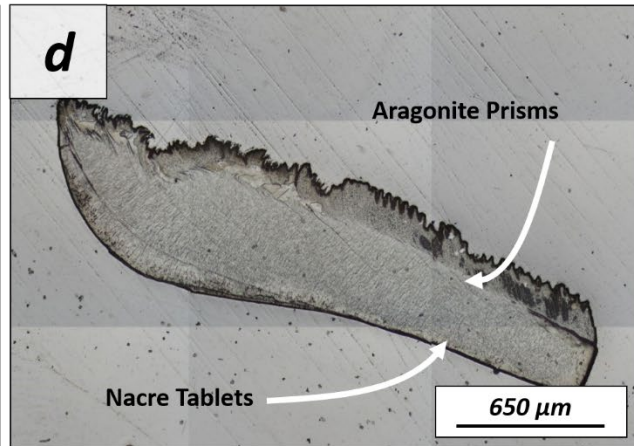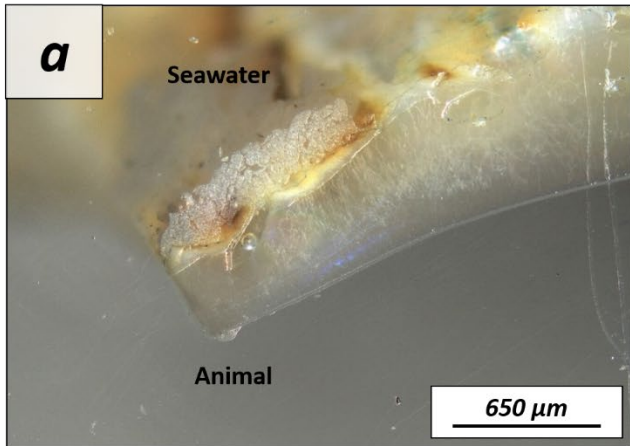
Figure A7. Laser confocal microscopy images of (a-c) pristine and (d-f) altered shells of *Haliotis ovina*. The shell is composed of two layers: a prismatic outer layer and a nacreous inner layer close to the animal soft tissue. While the nacreous layer shows no major structural change upon alteration, large calcite crystals can be observed in the prismatic layer after 6 months interaction with the burial fluid.

1110
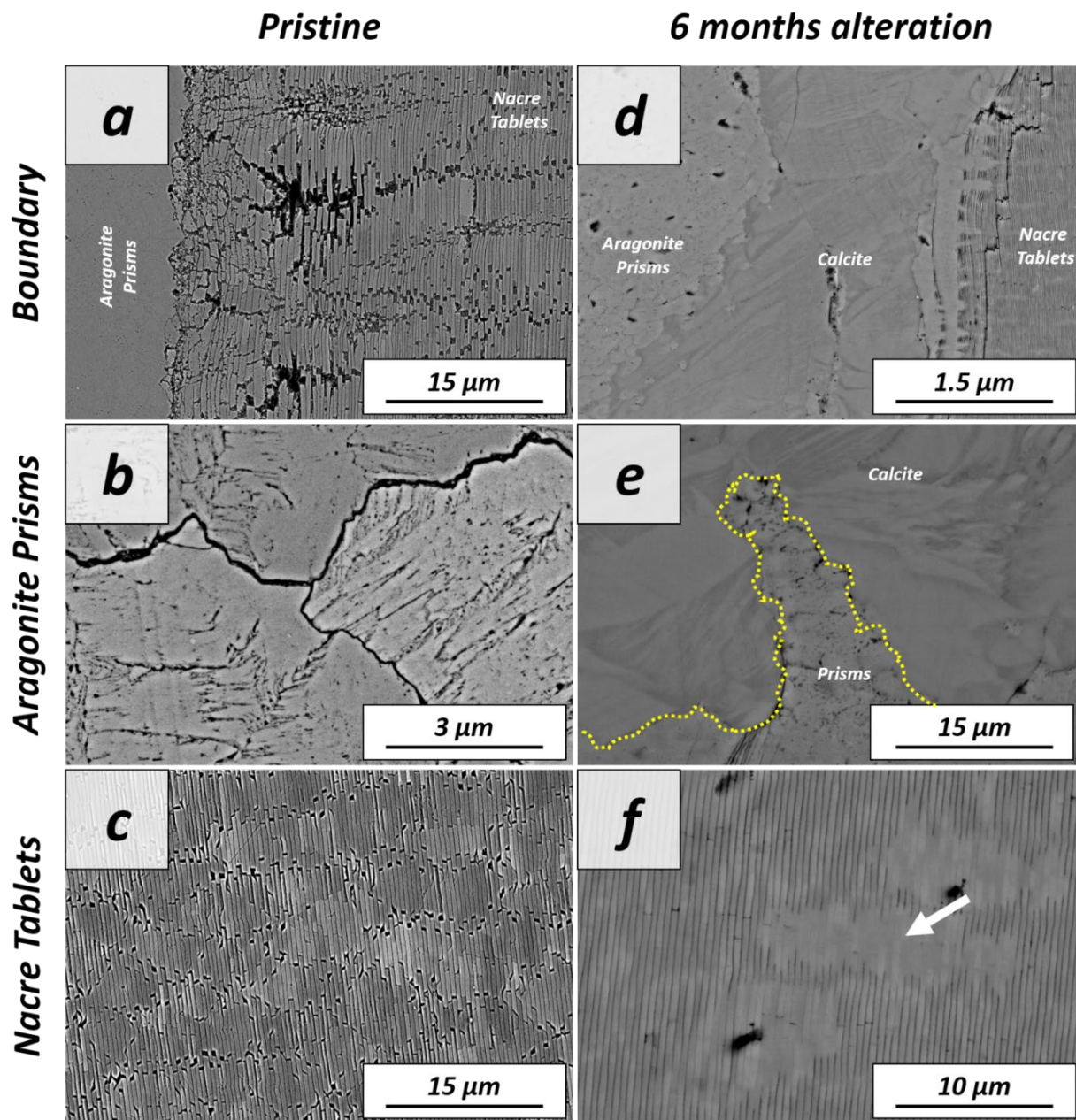
Figure A8. FE-SEM images depicting the internal structure of (a,c) pristine and of (d-f) altered shells of the gastropod *Haliotis ovina*. (a) *Haliotis ovina* shells consist of two layers: (b) An outer layer formed of aragonite prisms up to 3 micrometres in width and (c) an inner layer next to the soft tissue of the animal consisting of columnar assemblies of nacre tablets. (d-f) Hydrothermal alteration of *Haliotis ovina* shells for 6 months at 80°C in a burial fluid leads to the formation of new calcite crystals in the prismatic layer. These calcite crystals are concentrated at the interphase between the prisms and the nacre tablets. The aragonitic nacre tablets do not show transformation into calcite. However, tablet amalgamation is well observable as the edges and margins within stacks of tablets become blurred (white arrow in Fig A8d).
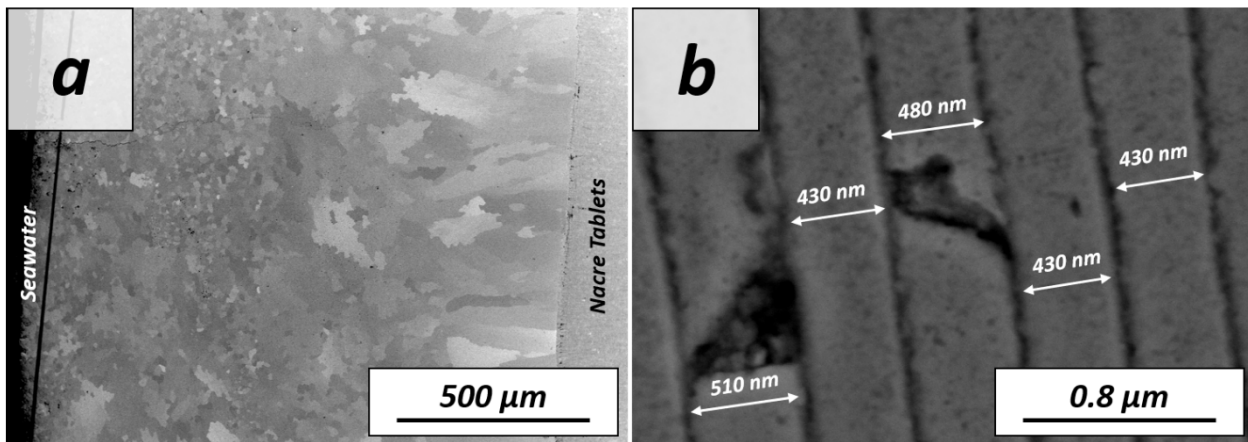
Figure A9. FE-SEM images showing the (a) prismatic and (b) nacreous layers of the shell of the gastropod *Haliotis ovina*. (a) Aragonitic prisms which build the outer layer of the shell are not similar in size. Small prisms form the outermost shell layers, while large prisms accumulate at the transition to the nacreous shell portion. (a, b) Aragonitic nacre tablet assemblies are next to the soft tissue of the animal. The tablets have a width in cross-section between 400 to 500 nm.
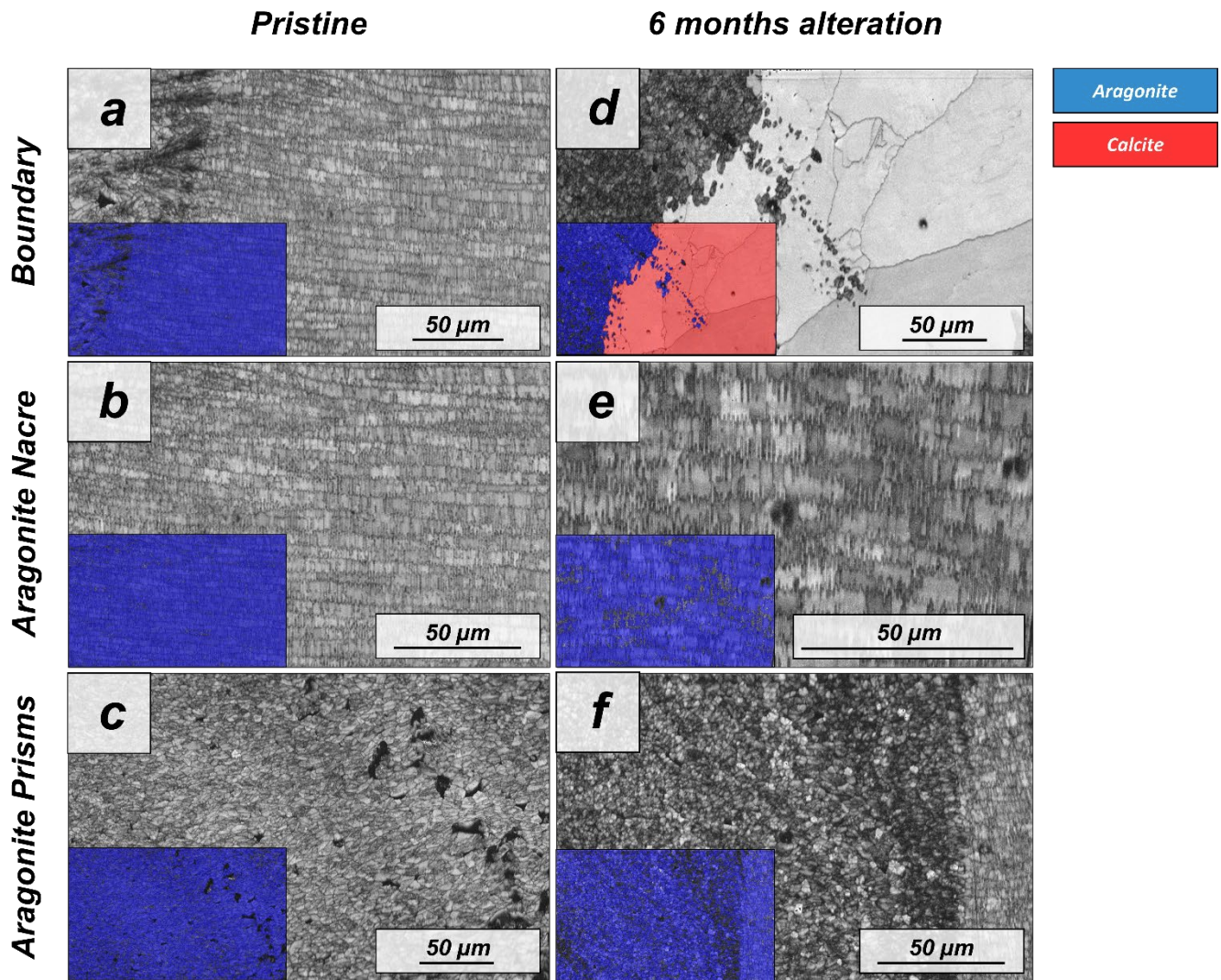
Figure A10. EBSD band contrast and phase maps illustrating differences in microstructure and mineralogy between the pristine and the most altered shells of *Haliotis ovina*; alteration lasted for 6 months and was done with a Mg-rich, burial-mimicking fluid at an alteration temperature of 80 °C. It is well visible that large parts of the prismatic layer are transformed to calcite, while the nacreous shell layer still consists solely of aragonite.

1135
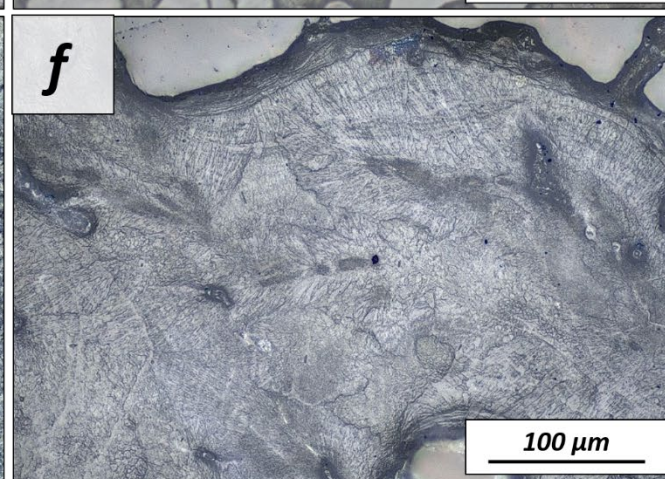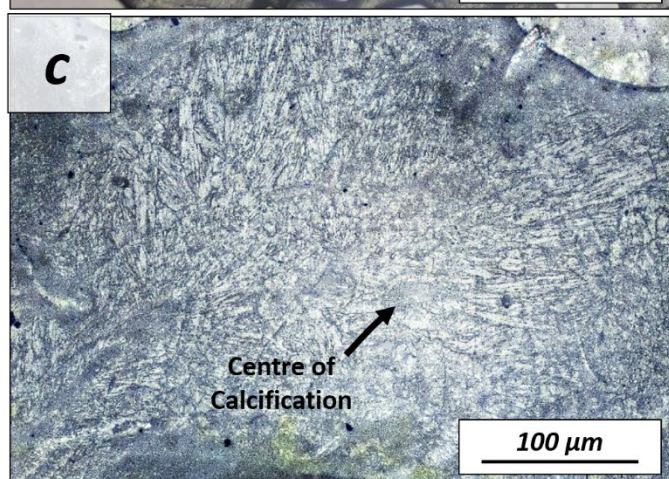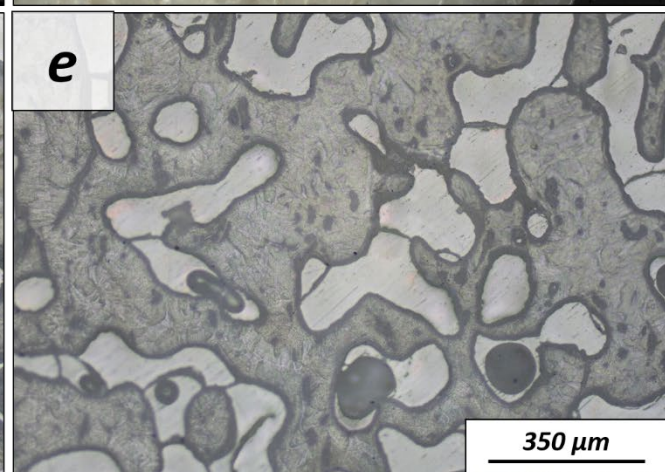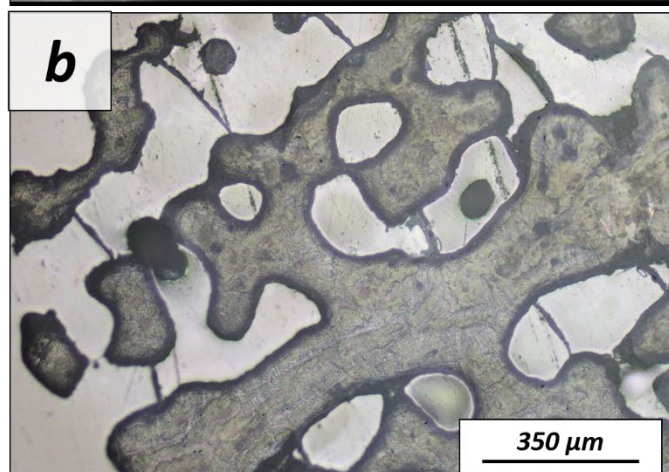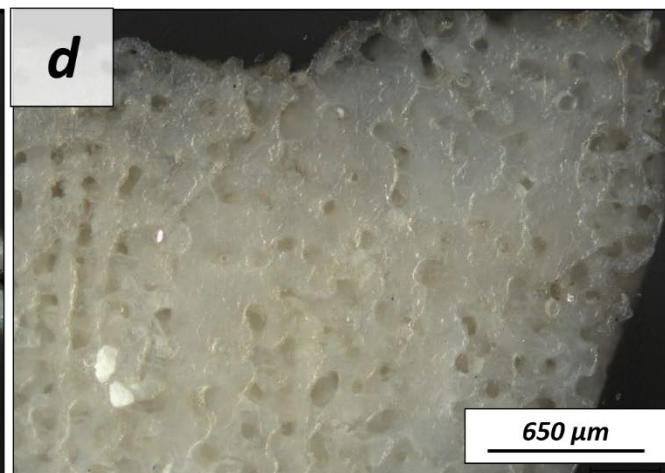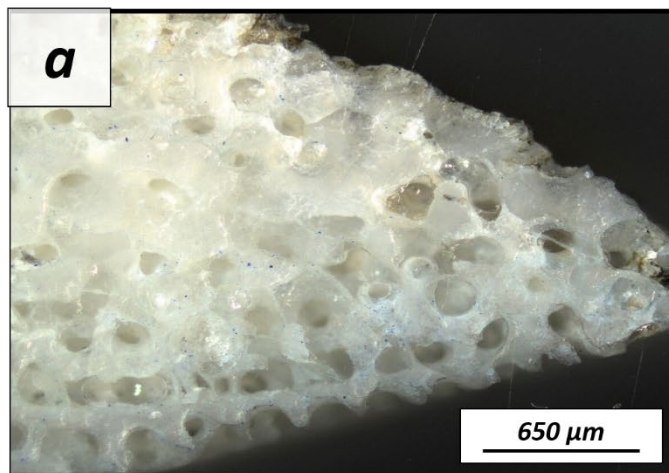
Figure A11. Laser confocal microscopy images of: (a-c) the pristine and the (d-f) altered skeleton of *Porites* sp. This coral species has a huge primary porosity, while the aragonitic hard tissue itself is densely mineralized (a to c). Aragonite acicles, needles and fibrils grow out of centres of calcification (a). Hydrothermal alteration for 6 months, at 80 °C in a Mg-rich fluid does not induce significant changes to the skeleton microstructure, as visible in Figs. A11d to A11f.

1140
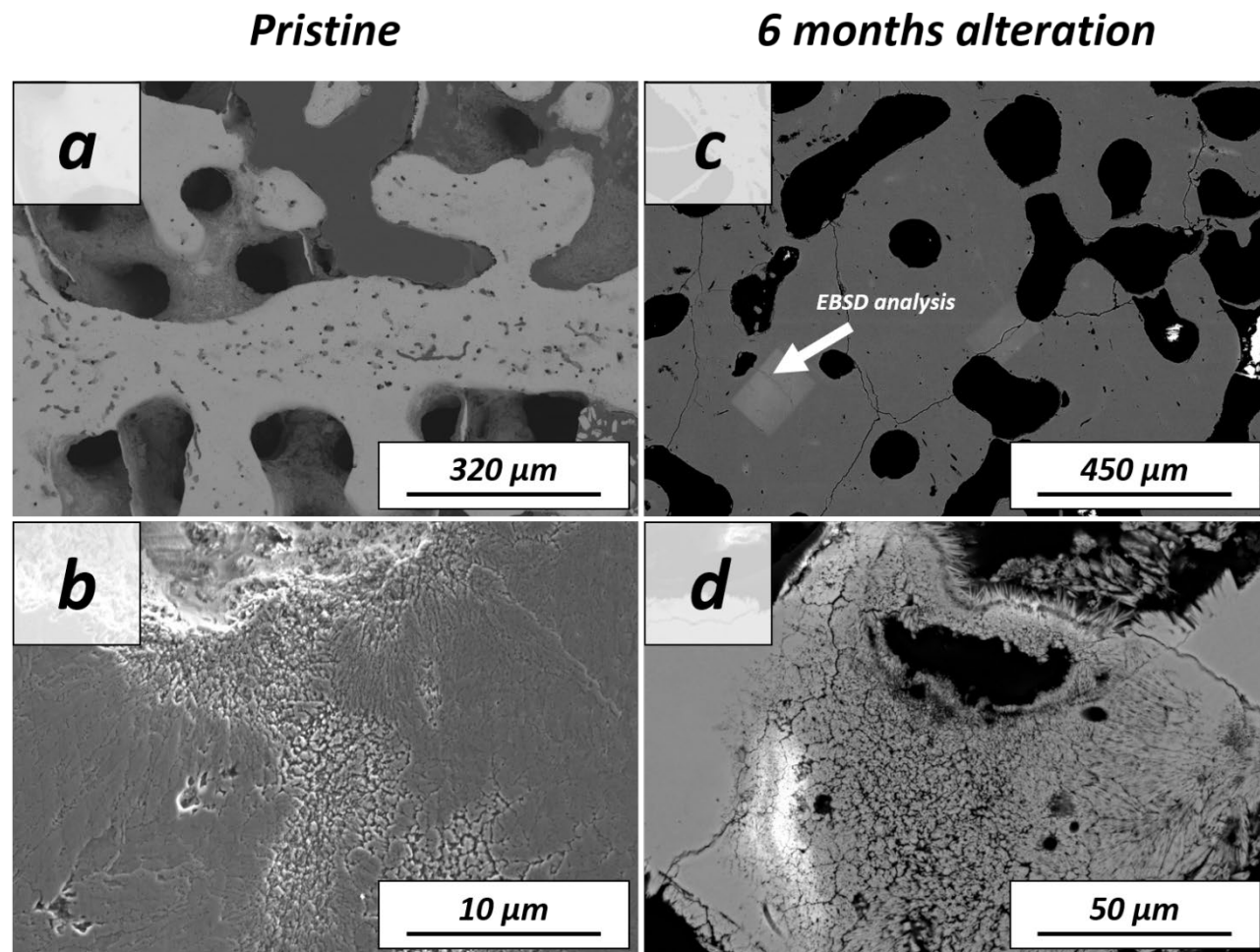
Figure A12. SEM images showing the (a,b) pristine and (c,d) altered skeletons of the coral *Porites* sp. The stony skeleton of *Porites* sp. has abundant intrinsic porosity within the mineralized units. The aragonite grows as fibrils outward from the centres of calcification. (c,d) The aragonitic microstructure of the coral *Porites* sp. is extremely resistant and undergoes no major

1145   changes upon hydrothermal alteration with a burial-mimicking fluid for 6 months at 80ºC according to SEM images.

Pristine   **6 months alteration**
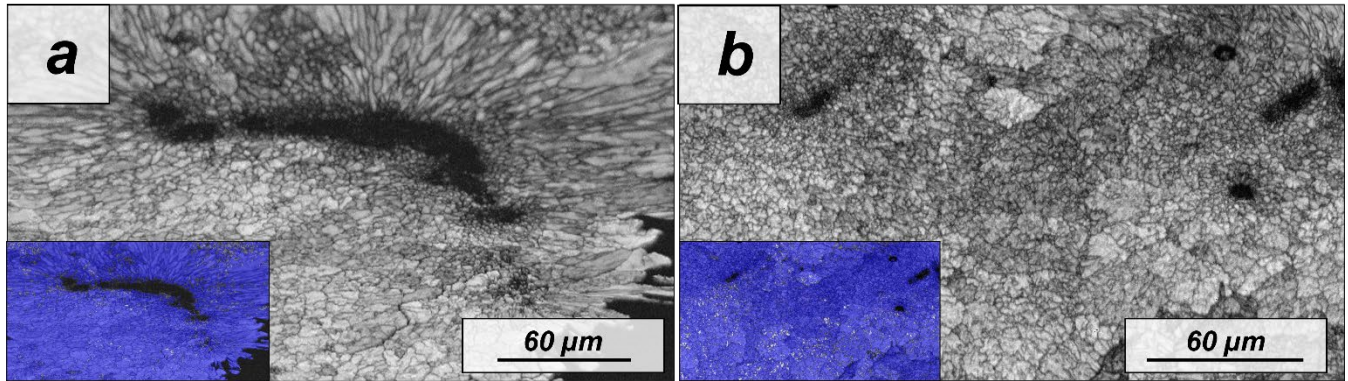
Figure A13. EBSD band contrast and phase maps illustrating the differences in microstructure and mineralogy between the pristine and the most altered skeletons of *Porites* sp.
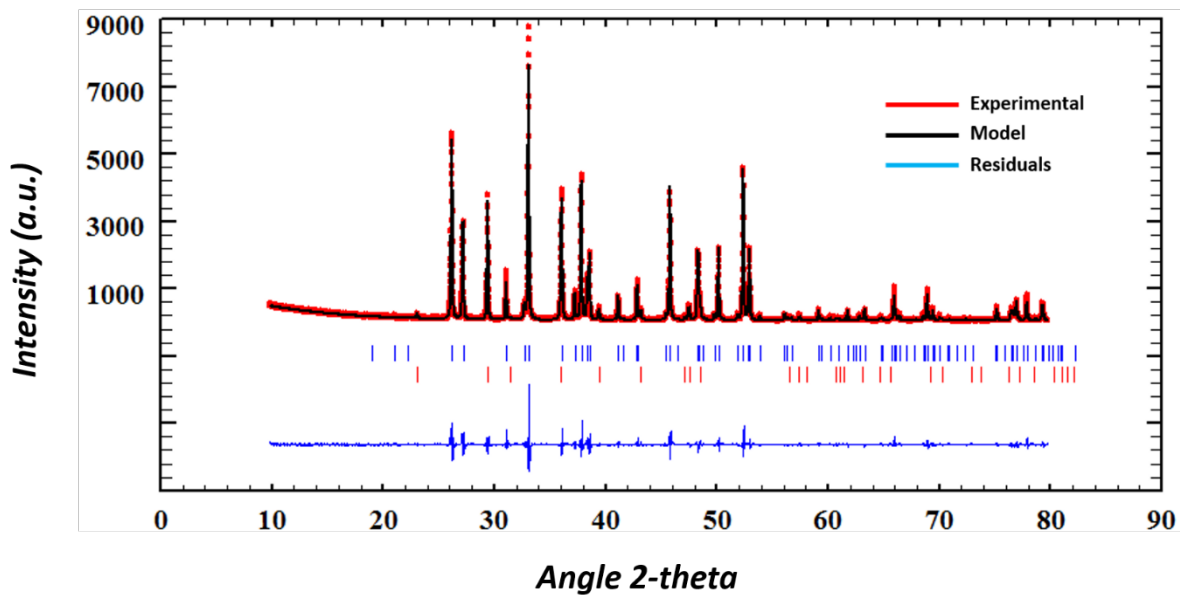
Figure A14. Exemplary Rietveld refinement plot for an altered *Haliotis ovina* sample (6 months, 80 °C in Mg-rich fluid). Red dots: data points, black line: calculated XRD profile, bottom blue line: difference between observed and calculated data, blue vertical bars: positions of aragonite diffraction peaks, red vertical bars: position of calcite diffraction peaks.